Forward Compton Scattering Amplitude as a Simultaneous Analytic Function of Complex Photon Mass and Energy*

Ashok suri
Stanford Linear Accelerator Center, Stanford University, Stanford, California 94305, and Division of Natural Sciences, University of California, Santa Cruz, California 95060
(Received 8 May 1970; revised manuscript received 8 February 1971)

The analytic structure of the virtual forward Compton scattering amplitude as a function of one and two complex variables is investigated for various combinations of variables which involve the virtual photon mass. This is done both by using the Deser-Gilbert-Sudarshan representation and by using the Feynman perturbation theory. The role and significance of complex Landau singularities is discussed. In general these are branch points, but it is found that at $t=0$ some of these become poles. The effect of these complex singularities and of overlapping cuts on the ordinary single-variable dispersion relations and the mass extrapolations in the vector-meson-dominance model is explained. Using the Cutkosky discontinuity formula for Feynman graphs, the analytic structure of the discontinuities across various normal threshold cuts of the non-Born-term part of this amplitude is deduced. One finds that the two-variable analyticity of the amplitude implies a single-variable analyticity for these discontinuities. It is shown that in general the inelastic structure functions W and $\overline{W}$ cannot be expected to have a simply determinable analytic structure. But under certain conditions W and $\overline{W}$ can be identified with boundary values of the discontinuities across the s- and u-channel normal threshold cuts in the virtual forward Compton scattering amplitude, respectively. This is used to show that the contribution to W and $\overline{W}$ from certain types of Feynman graphs under certain conditions are analytic functions of one complex variable, and only for such cases can one use crossing symmetry to relate the inelastic-electron-scattering structure functions and the annihilation structure functions. The motion of the Landau singularities of νW_2 is shown to provide a possible explanation for its observed rapid approach to "scaling" for finite but large final-state masses.

I. INTRODUCTION

In the recent literature on inelastic electron scattering, increasing use has been made of analytic continuations of the inelastic-electroproduction structure functions [see Ref. 1, especially Refs. 1a, 1b, and 1c] and single-variable dispersion relations in the virtual photon mass q^2 for the virtual forward Compton scattering amplitude[1e,1f] and for its integrated absorptive parts.[1g] Power-series expansions in q^2 for fixed center-of-mass energy s have been used in the analysis of experimental data on these electroproduction structure functions.[1h] The vector-meson-dominance model (VDM) depends crucially on "smooth" analytic continuations in the mass q^2,[1i-1k] and so do some theorems of current algebra.[1m] We would like to know the limitations and range of validity of all such analytic continuations, dispersion relations, and power-series expansions. For this purpose, we investigate the analytic structure of the virtual forward Compton scattering (VFC) amplitude T as an analytic function of one and two complex variables and demonstrate a method of deducing, in certain cases, the analytic structure of its discontinuities across fixed cuts and of the inelastic structure functions.

Our analysis is based on the Feynman perturbation theory,[2] and we only consider massive scalar particles. We ignore spin and renormalization, since these do not affect the position of the singularities on the physical sheet. However, the strength (residues of poles and discontinuities across cuts) and the nature of these singularities do depend on spin, renormalization, and the nature of the couplings. Besides these, renormalization can also affect the singularity structure on unphysical sheets. Our results therefore apply to the kinematic singularity-free invariant amplitude, and we hope that the physical-sheet analyticity is valid even if the perturbation theory fails[2a,3] (as in the case of strong interactions). In this paper we do not attempt any rigorous proofs, but simply demonstrate some important theorems and physical features relevant to the problem.

In Sec. II we collect the basic definitions used throughout the paper.

In Sec. III we start by giving a practical discussion of the Deser-Gilbert-Sudarshan (DGS) representation,[4] and show how one can deduce the analyticity of the VFC amplitude directly from this representation for any combination taken as the pair of independent variables. The results are tabulated in Table I. From our analysis we find

that the DGS representation implies the same analyticity for the full VFC amplitude as we obtain from the subsequent perturbative analysis. However, for a single-box diagram, we do get a larger domain of analyticity than implied by the DGS representation. This is because in the absence of knowledge of the detailed structure of the DGS spectral function, the DGS representation is incapable of showing an analytic continuation with complex singularities, except by giving an infinite cut along the whole real axis (which separates the whole complex plane into a pair of disjoint half planes). We show how to determine the DGS spectral function for an arbitrary Feynman graph, and use it to show that for the box diagram the DGS representation gives the same analytic structure as perturbation theory does for the absorptive part of the box graph. This analysis also demonstrates a practical technique of determining whether the contribution of a particular Feynman graph to the inelastic structure functions[5] "scales" or not in the Bjorken limit.[1]

In Sec. IV we use well-known techniques[2,6,7] to determine the analytic structure of the Feynman integral for the box diagram with unstable external legs at $t=0$. On the basis of it we conjecture results for the complete VFC amplitude in all orders consisting of all possible Feynman graphs. The proof of these conjectures is left to a subsequent paper. The off-mass-shell continuation is defined by the Feynman integral, and the physical boundary is determined by the Feynman prescription of giving an infinitesimal negative imaginary part to the masses of all internal legs which are presumed stable (the resonances can also be treated as stable particles for the purpose of determining the physical-sheet singularities[6i]). Fixing $t=0$ is found very useful in trying to generalize our analysis to all orders, because at $t=0$ the dual diagram[8] for the VFC amplitude is topologically similar to the dual diagram for the vertex function. Therefore the two amplitudes are required to have their Landau singularities similarly located (though their nature could be different). An analogous result does not hold for the second-type[9] or mixed singularities[7c] which are not determined by the usual dual diagrams. One expects[9a] that the pure second-type singularities in all orders stay away from the physical sheet and are located at the edges of the physical region (at $s=0, 4M^2$, and $u=0, 4M^2$). However, we cannot make any definite statements about the mixed second-type singularities.[7c]

We indicate why we expect that an analysis of all orders of Feynman perturbation graphs at $t=0$ will show that besides the Born-term poles, the only Landau singularities on the physical sheet of the

TABLE I. The single-variable analyticity of T obtained from the DGS representation.

The pair of independent variables	The slope and intercept of the integration line $\sigma=\beta\nu+z$	Single-variable analyticity of the forward Compton amplitude T		
		Fixed real variable	Complex variable	Analytic structure in the one complex variable implied by the DGS representation[a]
(z,ν)	slope $=\nu$	$z=z_R$	ν	Real analytic for $z_R<\mu^2$; cut along the whole real ν axis for $z_R>\mu^2$
	intercept $=z$	$\nu=\nu_R$	z	Real analytic for all ν_R
(z,s)	$\nu=s-M^2-z$	$z=z_R$	s	Real analytic for all $z_R<\mu^2$; cut along the whole real s axis for $z_R>\mu^2$
	z	$s=s_R$	z	Real analytic for $s_R<(M+\mu)^2$; cut along the whole real z axis for $s_R>(M+\mu)^2$
(ν,s)	ν	$\nu=\nu_R$	s	Real analytic for all ν_R
	$z=s-M^2-\nu$	$s=s_R$	ν	Real analytic for $s_R<(M+\mu)^2$; cut along the whole real ν axis for $s_R>(M+\mu)^2$
(z,ω)	$\nu=-\omega z$	$z=z_R$	ω	Real analytic for $z<\mu^2$; cut along the whole real ω axis for $z>\mu^2$
	z	$\omega=\omega_R$	z	Real analytic for all ω_R
(ν,ω)	ν	$\nu=\nu_R$	ω	Real analytic for all ν_R
	$z=-\nu/\omega$	$\omega=\omega_R\neq 0$	ν	Real analytic for all $\omega_R\neq 0$
(ω,s)	$\nu=-\omega(s-M^2)/(1-\omega)$	$\omega=\omega_R$	s	Real analytic for all ω_R
	$z=(s-M^2)/(1-\omega)$	$s=s_R$	ω	Real analytic for $s<(M+\mu)^2$; cut along the whole real ω axis for $s>(M+\mu)^2$

[a]Note: When there is a cut along the whole real axis, one may still be able to define T as an analytic function in the whole complex plane, but it will then have complex singularities.

complex q^2 plane for fixed $s = s_R + i\epsilon$ (or vice versa) are the s-independent normal q^2-threshold branch points (for real timelike $q^2 > 0$) and a set of complex anomalous singularities $q_\pm^2(s)$, which move with s, and correspond to the single-loop box or triangle reduced diagrams. In particular, this shows that the Landau singularities of the full VFC amplitude nearest to the origin and on the real plane are given by the lowest-order Feynman graphs. This is a reflection of a similar well-known result for the vertex function.[8e]

When all the external legs are stable (or when s is below the normal threshold) the VFC amplitude has only real singularities on the physical sheet. These real singularities are the Born-term poles (due to weakly connected Feynman graphs which separate into two graphs on cutting a single line), and the normal and anomalous branch points. When the external legs are unstable, some of these anomalous branch points move over into the complex plane to give the complex Landau singularities. We find that at $t = 0$ some of these anomalous branch points coalesce to form simple anomalous poles (which come from the strongly connected graphs). We demonstrate this explicitly for the single-loop box graph, and give reasons why we believe this need not be true in similar situations for arbitrary Feynman graphs. This structure has important implications for ordinary single-variable dispersion relations (with semi-infinite real cuts and poles) and for mass extrapolation in the vector-meson-dominance model.[1i-1k]

We find that ordinary single-variable dispersion relations can cease to exist either when left- and right-hand cuts overlap, giving a cut along the whole real axis, or when we get complex anomalous singularities. Thus fixed-ν dispersion relations in complex q^2 exist for all real ν, while fixed real q^2 dispersion relations in ν cease to exist for $q^2 \geq 4\mu^2[1 - (\mu^2/4M^2)]$. Similar results for other

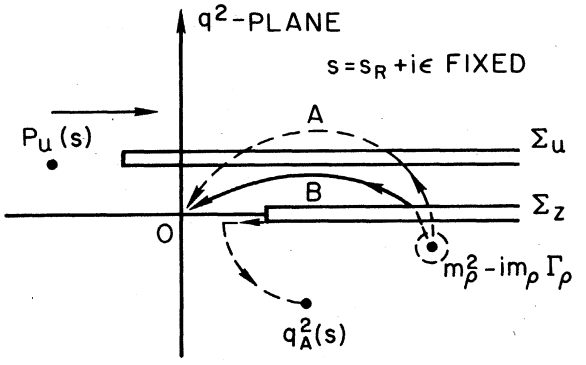

FIG. 1. The analytic structure of the virtual forward Compton scattering amplitude in the complex q^2 plane for fixed real s.

choices of variables are listed in Table I.

In order to study the mass extrapolation in the VDM, we consider the physical-sheet analytic structure (see Fig. 1) of the VFC amplitude in the complex q^2 plane for real s fixed above the threshold, i.e., $\mathrm{Re}\, s \geq (M+\mu)^2$, $\mathrm{Im}\, s \to 0+$. From Fig. 17(c) and our subsequent discussion, we will find that we have a real cut $\Sigma_z \equiv \{4\mu^2 \leq q^2 \leq \infty\}$ due to the normal q^2 threshold together with a moving (with s) overlapping cut $\Sigma_u \equiv \{\frac{1}{2}(s - 4M^2 + u) \leq \mathrm{Re}\, q^2 \leq \infty, \mathrm{Im}\, q^2 \to 0+\}$ due to the u-channel normal threshold, with the physical region squeezed between them. In addition we have the complex anomalous singularities like $q_A^2(s)$, the u-channel Born poles $P_u(s)$, and the vector-meson-resonance poles on the second sheet at $m_\rho^2 - im_\rho\Gamma_\rho$. VDM requires an analytic continuation of the VFC amplitude from the ρ pole to the origin. For small s_R, Σ_u overlaps Σ_z squeezing the physical region between them, and the above analytic continuation is not possible since the continuation path A leads off to the unphysical sheet in the $\epsilon \to 0+$ limit. But for large s_R this cut moves to the right exposing the physical boundary and the analytic continuation is possible along a path B. This is the well-known[1j] reason why VDM is expected to work for large real s only. Now the mass-extrapolation assumption for VDM amounts to dominating the absorptive part across the normal q^2 cut Σ_z by the ρ pole with a width (which parametrizes the effect of this cut), cutting off u-channel poles $P_u(s)$ by the form factor and ignoring the Σ_u cut due to its distance. But VDM also ignores the contributions of complex anomalous singularities. This we find to be unjustified because even though, at large real s, these anomalous singularities may have a small effect on the modulus of the VFC amplitude at $q^2 = 0$, due to their large (of order of s_R) distance from the origin, they can still have very significant effect on the phase of the amplitude (or its ratio of real to imaginary part). Related results for the case $t \neq 0$ have been recently obtained by Potter and Sullivan.[1k]

In contrast to the DGS representation, the advantage of our perturbative analysis is that we can deduce the single-variable analyticity of the discontinuities of the non-Born-term part (the strongly connected Feynman graphs) of the VFC amplitude across the various normal threshold cuts. The Born terms give nonanalytic δ-function contributions. The single-variable analyticity of the discontinuities is found as a straightforward consequence of the two-variable analyticity of the amplitude. These facts are apparent from the Cutkosky discontinuity formula,[2a,10] from which one can also show that the non-Born-term parts (nonresonant final states) of the inelastic structure functions are a boundary value of the discontinuity functions on

and only on the cut-free part of the real axis, when the mass of the undetected final state is kept fixed. These facts are explained further in Sec. V. There we also discuss the special class of graphs for which the inelastic structure functions can be analytically continued from the scattering region to the annihilation region.[1b, 1c, 11]

In a separate publication[11] we discuss an interesting application of our analysis which is based on the observation that the physical x-sheet anomalous singularities $x_i(s)$ of $W(s, x)$ rapidly approach their s-independent asymptotic position once s is large enough. We propose that this may provide an explanation of the rapid approach to "universality" of the inelastic-electron-scattering structure functions. A simple-minded discussion of the physical basis of this proposal is given in Secs. IV C and V.

Most of the sections of this paper can be read independently of each other. In particular we suggest Secs. IV C and V to those interested in practical applications of our analysis.

II. DEFINITIONS

The forward Compton scattering amplitude represents the process $\gamma N \to \gamma N$ when there is no four-momentum transferred from the photon to the nucleon. This process is shown in Fig. 2. For future reference we list the relevant kinematic variables below [our metric is $(1, -1, -1, -1)$ and $\hbar = c = 1$]:

(1) The photon mass is $q^2 \equiv z$.

(2) The nucleon mass is $P^2 = M^2$(fixed).

(3) The energy of the photon in the rest frame of the nucleon is proportional to $\nu \equiv 2q \cdot P$.

(4) The direct-channel center-of-mass energy equals

$$s \equiv (p_1 + p_2)^2 = (q + P)^2 = z + \nu + M^2.$$

(5) The momentum transfers are

$$t = (p_2 + p_4)^2 = (P - P)^2 = 0 \text{ (fixed)},$$

$$u = (p_2 + p_3)^2 = (P - q)^2 = z - \nu + M^2.$$

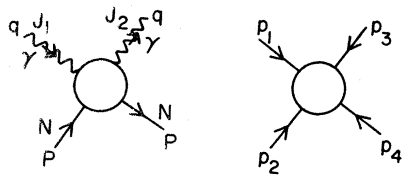

FIG. 2. The virtual forward Compton scattering amplitude.

These satisfy $s + u = 2z + 2M^2$.

(6) The scaling variables are

$$\omega = \frac{2q \cdot P}{-q^2} = -\frac{\nu}{z}$$

and

$$x \equiv \frac{z}{\nu} = -\frac{1}{\omega}.$$

If we keep $P^2 = M^2$ and $t = 0$ fixed, we know from Lorentz invariance that T is a function of two invariants. We choose these to be either the set (z, ν) or the set (z, s), and study the analytic structure of $T(z, \nu)$ and $T(z, s)$ as functions of complex z, ν, and s.

When the spins of the photon and the nucleon are considered, one finds that T is a multicomponent Lorentz tensor $T_{\mu\nu}^{(\alpha\beta)}$, where α and β are spinor indices and μ and ν are vector indices. Then one can use Lorentz invariance[2h, 21] to expand the tensor amplitude in terms of a complete set of linearly independent tensors $\{\mathfrak{L}_{\mu\nu}^{(\alpha\beta)}(i)\}$ formed out of q_μ, P_μ, $\gamma_\mu^{(\alpha\beta)}$, and $\epsilon_\mu^{(\alpha)}$, as follows:

$$T_{\mu\nu}^{(\alpha\beta)} = \sum_i \mathfrak{L}_{\mu\nu}^{(\alpha\beta)}(i) T_i. \tag{1}$$

Here the coefficients T_i are scalar functions of linearly independent invariants, and we call these invariant amplitudes. These are chosen to be free of kinematic singularities, which can be discovered by applying conservation laws like four-momentum conservation and gauge invariance.[1i, 11]

It is well known[2a, 2c] that the analytic structure of the invariant amplitudes is the same as that of a corresponding amplitude with all spins ignored. That spin is an "inessential complication" in the study of analyticity is most easily understood in terms of the Feynman graphs in which spin just adds extra momentum-dependent terms in the numerator of the integrand, but does not affect the denominators whose zeros give the usual Landau[6] and second-type singularities.[9] On the other hand, it should also be clear that spin will be very important in the study of the asymptotic behavior[2a] which is an input for the dispersion relations. This will not concern us in the present paper. However, when discussing specific cases we should remember that these spin factors can lead to cancellations within a particular Feynman integral, or between different ones in a sum of Feynman integrals. From now on we shall ignore all the spin factors and only consider scalar particles. Hence, our results will only apply to the kinematic singularity-free invariant amplitudes. In the same spirit we will also assume as usual that the infrared and ultraviolet divergences have been removed by a suitable cutoff.

III. RESULTS FROM THE DGS REPRESENTATION

Using the Lehmann-Symanzik-Zimmermann (LSZ) reduction formulas,[2h] the forward Compton scattering amplitude can be defined in three ways (ignoring spin):

$$T_R(q,P) \equiv i\int d^4x\, e^{iq\cdot x}\langle P|\theta(x_0)[J_1(x),J_2(0)]|P\rangle,$$

$$T_A(q,P) \equiv -i\int d^4x\, e^{iq\cdot x}\langle P|\theta(-x_0)[J_1(x),J_2(0)]|P\rangle, \tag{2}$$

or

$$T_T(q,P) \equiv i\int d^4x\, e^{iq\cdot x}\langle P|T_+(J_1(x)J_2(0))|P\rangle,$$

where $J_1(x)$ and $J_2(x)$ are local electromagnetic currents and T_+ the positive time-ordering operator. For a stable nucleon these definitions agree for various physical values of the four-momenta q and P. This is seen as follows:

$$\begin{aligned} T_+(J_1(x)J_2(0)) &= \theta(x_0)[J_1(x),J_2(0)]+J_2(0)J_1(x) \\ &= -\theta(-x_0)[J_1(x),J_2(0)]+J_1(x)J_2(0). \end{aligned} \tag{3}$$

Therefore

$$\begin{aligned} T_T(q,P)-T_R(q,P) &= i\int d^4x\, e^{iq\cdot x}\langle P|J_2(0)J_1(x)|P\rangle \\ &= i\sum_n (2\pi)^4\delta^{(4)}(q-P+P_n)\langle P|J_2(0)|n\rangle\langle n|J_1(0)|P\rangle. \end{aligned} \tag{4}$$

Energy conservation and the stability of the physical nucleon of momentum P ($P^0\geq 0$) forbids it to decay into a physical single particle of momentum q ($q^0\geq 0$) and another system of momentum P_n ($P^0\geq 0$). Therefore $P_n=0$, i.e., the only intermediate state allowed is the vacuum. But $\langle P|J_2(0)|\Omega\rangle=0$ from the LSZ assumptions. Therefore, in the physical region of the s channel [$q^0>0$, $(q\cdot P)^2\geq q^2P^2$], $T_T(q,P)=T_R(q,P)$. Similarly, in the physical region for the (crossed) u channel [$q^0<0$, $(q\cdot P)^2\geq q^2P^2$], $T_T(q,P)=T_A(q,P)$.

This shows that in the appropriate physical regions T_T coincides with $T_{R,A}$. For unphysical (and complex) values of the momenta one must define the amplitude T by means of an analytic continuation.[2m,2n] Then the functions T_T, T_R, and T_A will simply be different boundary values in the appropriate regions of this unique analytic continuation T. To seek this analytic continuation it is convenient to start with T_R or T_A rather than T_T, since the locality of the retarded (or advanced) commutator (i.e., vanishing at space-like separations) allows its Fourier transform to have a large domain of analyticity.[2] On the other hand, it is perfectly possible to arrive at this unique analytic function T by analytically continuing any representation for the scattering amplitude which has the suitable analyticity and agrees with T_T in the physical regions. This fact will be used in our subsequent discussions in this section. We should observe that even though the Feynman perturbation theory is derived using the form $T_T(q\cdot P)$, the analytic structure obtained by analyzing connected Feynman diagrams reflects the analytic structure of the retarded (or advanced) commutator. This is because Feynman graphs involve positive-energy particles and conserve four-momentum, so that the extra terms $J_2(0)J_1(x)$ or $J_1(x)J_2(0)$ are not seen in the diagrams contributing to the respective channels. To be precise, the connected Feynman diagrams correspond to the connected part of the retarded (or advanced) commutator defined by

$$\theta(\pm x_0)\langle P|[J_1(x),J_2(0)]|P\rangle_{\text{connected}} \equiv \theta(\pm x_0)\langle P|[J_1(x),J_2(0)]|P\rangle - \theta(\pm x_0)\delta^{(4)}(P-P')\langle\Omega|[J_1(x),J_2(0)]|\Omega\rangle. \tag{5}$$

The term $\theta(\pm x_0)\delta^{(4)}(P-P')\langle\Omega|[J_1(x),J_2(0)]|\Omega\rangle$ corresponds to the disconnected graphs shown in Fig. 3(a).

When discussing analytic continuations we will be interested mainly in the cut structure of the amplitude in the complex planes. Since pole graphs do not affect such structures, we shall ignore them in all our discussions.

Let us now consider the amplitudes $T_R(q,P)$ and $T_A(q,P)$. Using the identity[2h,2j]

$$e^{iq_0x_0}\theta(\pm x_0) \equiv \pm(2\pi i)^{-1}\int_{-\infty}^{\infty} dq_0'\, e^{iq_0'x_0}(q_0'-q_0\mp i\epsilon)^{-1}$$

(or a subtracted version), it is easy to show that T_R is analytic in the upper half q_0 plane and T_A is analytic in the lower half q_0 plane. We can define a function T which equals T_R in the upper half plane and T_A in the lower half plane. The two half planes are separated along the whole real axis, with the discontinuity

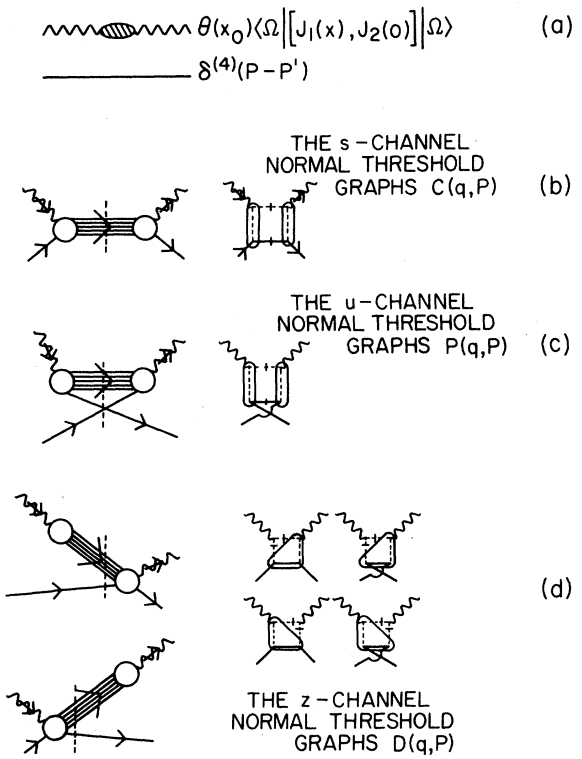

FIG. 3. The unitarity and discontinuity diagrams.

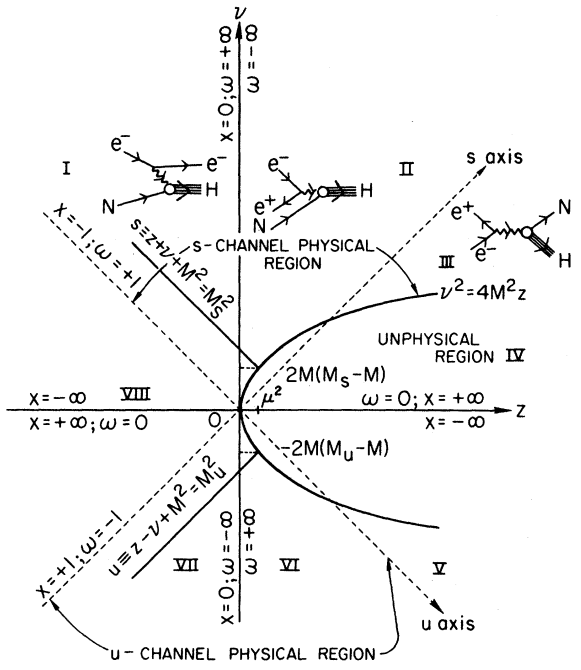

FIG. 4. The various physical regions for the forward Compton amplitude. The experimentally accessible areas show the different reactions which involve parts of the forward Compton amplitude in the definition of its inelastic form factors. (H is any hadronic system.)

in T across the real q^0 axis being the absorptive part of T which equals

$$A(q,P)\equiv\int_{-\infty}^{\infty}d^4x\,e^{iq\cdot x}\langle P|[J_1(x),J_2(0)]|P\rangle=T(q_0+i\epsilon)-T(q_0-i\epsilon)=T_R(q_0)-T_A(q_0)\,. \tag{6}$$

In the case in which this discontinuity vanishes across some finite interval of the real q^0 axis, we can analytically connect T_R and T_A across this segment, and then T defines a real analytic function of q^0; otherwise not. On the other hand, if this absorptive part is nonzero along the whole real q^0 axis, then T_R and T_A are not analytically connected. However, we will see from the analysis of the Feynman graphs that one may still be able to define an analytic continuation of T_R (and a different one for T_A) into the lower half plane, but this continuation will have branch points in the complex plane (and corresponding complex cuts) and will not be a real analytic function. Here again we must remember that as long as we can find an analytic function which equals T_R or T_A in the appropriate physical regions, it is a perfectly legitimate analytic continuation into the unphysical region, though the domains of different analytic continuations would be different. This fact will be very useful in understanding the Compton amplitude for $q^2>0$.

To understand the physical significance of the absorptive part $A(q,P)$, we put in a complete set of physical (in or out) states, use translational invariance, and integrate to get

$$A(q,P)=(2\pi)^4\sum_n[\delta^{(4)}(q+P-P_n)\langle P|J_1(0)|n\rangle\langle n|J_2(0)|P\rangle-\delta^{(4)}(q-P+P_n)\langle P|J_2(0)|n\rangle\langle n|J_1(0)|P\rangle]\,. \tag{7}$$

Now, for all q^2 in the s-channel physical region ($q^0>0$, $P^0>0$, $P_n^0\geq 0$, see Fig. 4), energy conservation and stability of the nucleon make the second term vanish, so we get for all q^2

$$A(q,P)_{\text{physical}}=(2\pi)^4\sum_n\delta^{(4)}(q+P-P_n)\langle P|J_1(0)|n\rangle\langle n|J_2(0)|P\rangle\,. \tag{8}$$

The various parts of this commutator correspond to the various classes of connected unitarity diagrams C, P, and D shown in Fig. 3. Its disconnected part [Fig. 3(a)] is not needed for the present considerations. These parts are real quantities defined as

$$
\begin{aligned}
C(q,P) &= (2\pi)^4 \sum_k \delta^{(4)}(q+P-P_k)\langle P|J_1(0)|k\rangle_c \langle k|J_2(0)|P\rangle_c, \\
D(q,P) &= (2\pi)^4 \sum_l \delta^{(4)}(q-P_l)[\langle \Omega|J_1(0)|l\rangle_c \langle l,P|J_2(0)|P\rangle_c + \langle P|J_1(0)|P,l\rangle_c \langle l|J_2(0)|\Omega\rangle_c], \\
P(q,P) &= (2\pi)^4 \sum_m \delta^{(4)}(q-P-P_m)\langle \Omega|J_1(0)|P,m\rangle_c \langle m,P|J_2(0)|\Omega\rangle_c, \\
A(q,P) &= C(q,P) + D(q,P) \pm P(q,P),
\end{aligned}
\tag{9}
$$

where the subscript c denotes the connected part of the matrix element. From Figs. 3(b), 3(c), and 3(d) we observe that the unitarity diagrams for C, P, and D are topologically similar to the Cutkosky discontinuity diagrams for the discontinuities across various s-, u-, and z-channel normal threshold cuts, respectively. The relationship between C, P, D and $\mathrm{disc}_s T$, $\mathrm{disc}_u T$, $\mathrm{disc}_z T$, respectively, will be discussed later.

Using the LSZ reduction techniques it is easy to show the crossing relation

$$C(q,P) = \pm P(q,-P), \tag{10a}$$

where the (+) or (−) sign refers to a boson or a fermion target $|P\rangle$, respectively, reflecting the Pauli principle. For $q^0>0$ and $q^2<0$, C is like the structure function W for inelastic electron scattering ($e^- + N \to e^- + \text{anything}$). For $q^0>0$ and $q^2>0$, P is like the annihilation structure function $\overline{W}$ for the reaction ($e^+e^- \to N + \text{anything}$). Its clear that to use this crossing relation we need to analytically continue the two sides of the equation to common domains. If the existence of such an analytic continuation can be established, then it can be used to connect inelastic-electron-scattering and annihilation structure functions. The regions in which these functions are nonzero are shown in Fig. 4. In region I, only C contributes. In region II, $(C+D)$ contributes. In regions III, IV, and V $(C+D+P)$ contributes. In region VI, $(P+D)$ contributes. In region VII, P contributes, and in region VIII, none contribute and thus the commutator must vanish. This is because kinematics requires that C contribute for $s \geq 0$ (in fact M^2), that P contribute for $u \geq 0$ (and $z \geq 0$, but may be analytically continued into region VII keeping u fixed), and that D contribute for $z \geq 0$. We should observe that C, D, and P cannot vanish identically in any finite subregion of the unphysical region IV if they are analytic functions. But this does not restrict the value of their sum, which represents the full commutator and need not be analytic. A similar remark applies to regions III and V. Thus the vanishing of the sum $(C+D+P)$ in regions III, IV, and V (as indicated by Bjorken's analysis[1b,1d,1f] for the asymptotic-limit functions), together with analyticity, could be expected to impose rather strong restrictions on the functional form of C, D, and P. Since the J's are Hermitian boson currents, we can use Eqs. (6) and (8) to obtain an additional crossing relation

$$A(q^2,\nu) = -A(q^2,-\nu). \tag{10b}$$

To study the support of the absorptive part $A(q,P)$, it is convenient to use the DGS representation[4] which is derived on the following assumptions:

(1) microcausality, $[J_1(x), J_2(0)] = 0$ for all $x^2<0$ (spacelike);

(2) rapidly vanishing asymptotic behavior in α for

$$G(\alpha,\beta) \equiv \iint_{-\infty}^{\infty} d(x^2)d(Px)e^{-i\alpha x^2}e^{-i\beta(P\cdot x)}\langle P|[J_1(x),J_2(0)]|P\rangle \tag{11}$$

(we shall assume the unsubtracted form);

(3) T, P, or C invariance.

Nakanishi[4] has shown that every connected Feynman diagram satisfies a DGS representation, so that we should expect the results obtained from the DGS representation to be valid for each perturbation diagram. This is discussed further at the end of this section.

The DGS representation for the Fourier transform of a causal commutator states that

$$
\begin{aligned}
A(q,P) &\equiv \int d^4x\, e^{iq\cdot x}\langle P|[J_1(x),J_2(0)]|P\rangle \\
&= \int_{-1}^{1} d\beta \int_{-\beta^2P^2}^{\infty} d\sigma\, \epsilon(P\cdot q+\beta P^2)\delta(q^2+2\beta q\cdot P-\sigma)\sum_{n=0}^{N} H_n(\sigma,\beta)(P\cdot q+\beta P^2)^n,
\end{aligned}
\tag{12}
$$

where the function

$$\epsilon(x) = \begin{cases} +1 & \text{if } x>0 \\ -1 & \text{if } x<0. \end{cases}$$

The DGS spectral function $H(\sigma,\beta)$ is real, irrespective of the nature of the currents, because of T, P, or C invariance. The terms for $n>0$ correspond to terms in A which do not vanish as $|\nu|\to\infty$ for fixed z or $|z|\to\infty$ for fixed ν [where we express the polynomials in z by those in ν using their linear dependence due to $\delta(z+\nu-\sigma)$].[4d,4i,4j] For example, such terms can arise when the spin is not ignored. They would also occur when the commutator has Schwinger terms [since the Fourier transform of $(d^n/d(x^2)^n)\delta(x^2)$ is $(q^2)^n$]. Using crossing symmetry of the whole Compton amplitude (which requires symmetry under $\nu\to-\nu$), we can also show that $H(\sigma,-\beta)=H(\sigma,\beta)$.

We will be concerned with the case when the nucleon is massive and stable and we will ignore the subtraction terms, since they are known not to affect the analytic structure of the matrix elements. With these restrictions we can write (using our notation)

$$A(q,P)\equiv\int d^4x\,e^{iq\cdot x}\langle P|[J_1(x),J_2(0)]|P\rangle=\int_{-1}^{1}d\beta\int_0^\infty d\sigma\,\epsilon(\tfrac{1}{2}\nu+\beta M^2)\delta(z+\beta\nu-\sigma)H(\sigma,\beta). \tag{13}$$

The physical region in the real (z,ν) plane and the support of the spectral function $H(\sigma,\beta)$ in the real (σ,β) plane are shown in Figs. 4 and 5.

From their representation for $A(z,\nu)$, DGS are also able to derive a representation for T_R which is

$$T_{R,A}(q,P)=\int_{-1}^{1}d\beta\int_0^\infty d\sigma\,\frac{H(\sigma,\beta)}{z+\beta\nu-\sigma\pm i(\frac{1}{2}\nu+\beta M^2)\epsilon}+P(z,\nu), \tag{14}$$

where $P(z,\nu)$ is a real polynomial in z and ν.

The support of $H(\sigma,\beta)$ is deduced from the behavior of the commutator in the physical region. The physical region (where energy $\geq$ mass) is $\nu^2\geq 4M^2z$. The s-channel reactions lie in $s\equiv z+\nu+M^2\geq {M_s}^2$ and the u-channel reactions in $u=z-\nu+M^2\geq {M_u}^2$. For $M_s-M>0$ and $M_u-M>0$, these two regions are disjoint and this nucleon stability condition is crucial to our analysis (if these conditions are violated the analyticity is reduced drastically). The support Σ of $H(\sigma,\beta)$ is bounded by $-1\leq\beta\leq 1$, $\sigma\geq 2\mu M\beta+\mu^2$, and $\sigma\geq -2\mu M\beta+\mu^2$, assuming that $M_s=M_u=(M+\mu)^2$ where μ is the pion mass. Σ is shown in Fig. 5.

For every point in the (z,ν) plane the absorptive part $A(z,\nu)$ receives a contribution from the integral along the line in the (σ,β) plane given by the equation

$$z+\beta\nu-\sigma=0.$$

The parabola $\nu^2=4M^2z$ generates a set of lines in the (σ,β) plane which have as their envelope the parabola $\sigma=-\beta^2M^2$. The part of the line $s=z+\nu+M^2={M_s}^2$ in the physical region generates a pencil of lines through $(\sigma=M^2-{M_s}^2,\ \beta=-1)$, lying between tangents of positve slope and the line $\beta=+1$. Similarly, the line $u=z-\nu+M^2={M_u}^2$ gives the tangent to $\sigma=\beta^2M^2$ through $(\sigma=M^2-{M_u}^2,\ \beta=+1)$. All the lines generated by points in $\nu^2\geq 4M^2z$ intersect the parabola (or at least touch it) and the ϵ function changes sign inside the parabola (or at the point of contact) where $H(\sigma,\beta)$ vanishes. Also, in the support of $H(\sigma,\beta)$, $\epsilon(\frac{1}{2}\nu+\beta M^2)=\epsilon(\nu)$ for ν lying in the physical region of the (z,ν) plane.

Using the fact that due to the stability of the nucleon the s-channel physical region [where the term $\langle P|J_1(x)J_2(0)|P\rangle$ contributes] is disjoint from the u-channel physical region [where the term $\langle P|J_2(0)J_1(x)|P\rangle$ contributes], DGS show that one can write

$$T_T(q,P)=\int_{-1}^{1}d\beta\int_0^\infty d\sigma\,\frac{H(\sigma,\beta)}{z+\beta\nu-\sigma+i\epsilon} \tag{15}$$

To see the cut structure, we can write

$$T_T(z,\nu)=-\int_0^1 d\beta\int_{-z}^{\infty}d\nu'\,\frac{H(z+\nu',\beta)}{\nu'-\beta\nu-i\epsilon}$$

$$+\int_{-1}^{0}d\beta\int_{-\infty}^{z}d\nu'\,\frac{H(z-\nu',\beta)}{\nu'+\beta\nu+i\epsilon}, \tag{16}$$

whose imaginary part is given by

$$-\frac{1}{\pi}\,\mathrm{Im}\,T_T(q,P)=\int_{-1}^{1}d\beta\int_0^\infty d\sigma\,\delta(z+\beta\nu-\sigma)H(\sigma,\beta). \tag{17}$$

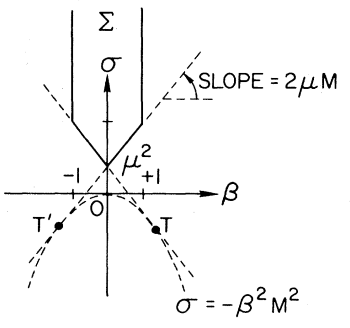

FIG. 5. The support Σ of the DGS weight function $H(\sigma,\beta)$.

We see that the DGS representation for $T_{R,A}$ defines a function which is analytic in the physical region [since there the sign of $(\frac{1}{2}\nu+\beta M^2)$ is fixed], but due to the presence of $i(\frac{1}{2}\nu+\beta M^2)\epsilon$, it cannot be continued to unphysical values of ν since $(\frac{1}{2}\nu+\beta M^2)$ can go through a zero and change sign. On the other hand, the representation obtained for T_T is continuable to the unphysical ν regions, provided $\mathrm{Im}T_T$ vanishes over a real interval in ν. To determine the support of $\mathrm{Im}T_T$, we use the fact that the nonvanishing contribution to the integral defining $\mathrm{Im}T_T$ comes from the intersection of the line $z+\beta\nu-\sigma=0$ with the support of $H(\sigma,\beta)$. From Fig. 6 we observe that for arbitrary fixed real ν and a variable z (or for z fixed less than μ^2 and ν variable), we can always find a pencil of such lines corresponding to a real z interval (or real ν interval, respectively), which do not intersect the support and therefore give a vanishing value of $\mathrm{Im}T_T$. In such cases the DGS representation for T_T defines a real analytic function of z for arbitrary fixed real ν with a cut along a part of the real z axis. Similarly, for fixed real $z<\mu^2$ we get a real analytic function of ν. But if we fix $z>\mu^2$, then the line $z+\beta\nu-\sigma=0$ always intersects the support for all real ν, and in general we will get a nonzero $\mathrm{Im}T_T$ for all real ν. In this case we do not have a real analytic function of ν, but instead a function which has a cut along the entire real axis, and the DGS representation for T_T can not be used to continue in ν from the upper half plane to the lower half plane. However, as we shall see in the analysis of Feynman graphs, we may still be able to find an analytic continuation of the amplitude from the upper half ν plane to the lower half ν plane, but this continuation will have complex branch points and, correspondingly, cuts in the complex plane. At this point we should note that in the case $z>\mu^2$, the nonvanishing of $\mathrm{Im}T_T$ for all real ν may not imply the nonvanishing of A for all real ν. This is because, for certain ν in the unphysical region, $\epsilon(\frac{1}{2}\nu+\beta M^2)$ can change sign on $z+\beta\nu-\sigma=0$ inside the support and so may cause the integral for A to vanish.

A similar analysis in Fig. 7 shows that for fixed $s>(M+\mu)^2$ the amplitude is not a real analytic function of z, and for fixed $z>\mu^2$ the amplitude is not a real analytic function of s. Of course, below these thresholds (which are the lower bounds on actual thresholds) we do get the amplitude to be a real analytic function of one variable. The reason is that for fixed s as we vary z, the σ intercept of the integration line rises while its slope decreases and [for, say, $s>(M+\mu)^2$] this can cause the integration line to intercept the support for all real z. In fact we observe that whenever a variable is such that varying it can cause this intercept to rise simultaneously with the falling slope, we can expect to get a nonreal analytic function (above the threshold for the fixed variable). On the other hand, if the intercept falls simultaneously with the falling slope, then we may expect a real analytic function. Using these rules, we can analyze the am-

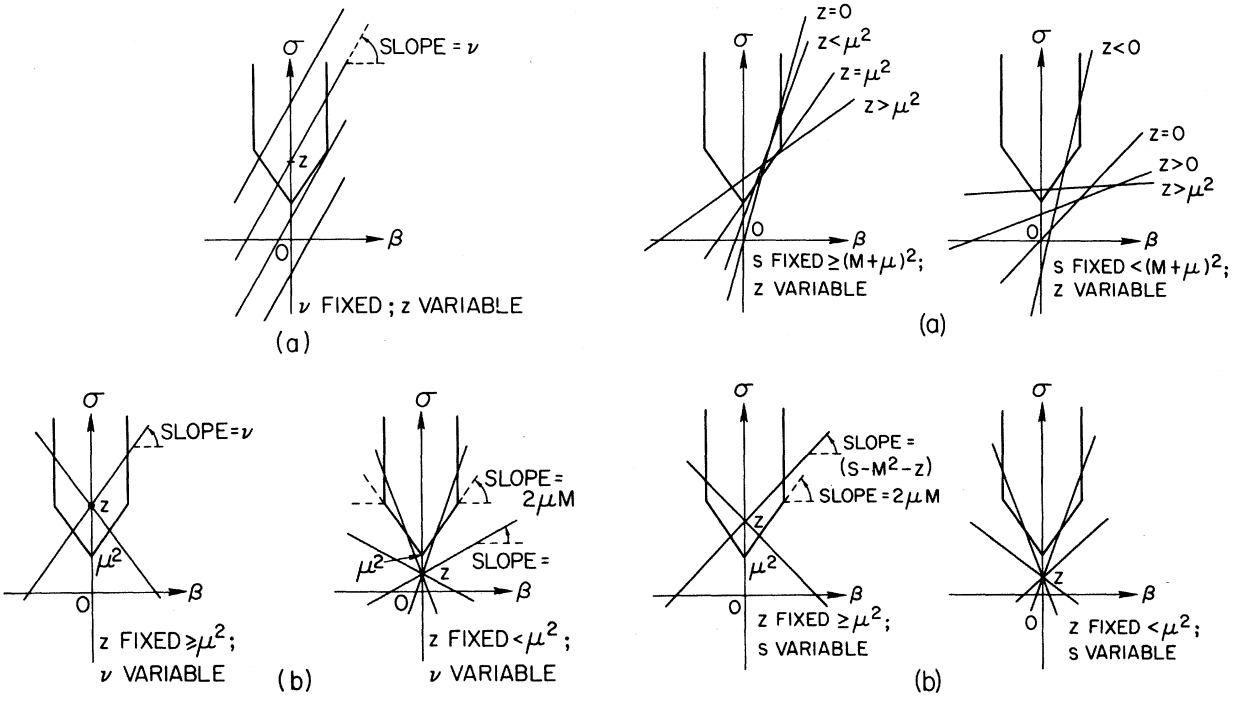

FIG. 6. The integration line $z+\beta\nu-\sigma=0$ for various z and ν.

FIG. 7. The integration line $z+\beta(s-M^2-z)-\sigma=0$ for various z and s.

plitude for any combination of a pair of invariant variables and the results are indicated in Table I.

We thus see that the representation for T_R derived from the DGS representation for A defines an analytic function in the physical region, but does not provide an analytic continuation of $T_{R,A}$ to the unphysical regions. Instead the representation for T_T is in a continuable form and the two agree on the various physical regions. Since T is defined to be the analytic continuation to the unphysical region of the physical-region amplitude (T_R or T_T), we choose the DGS representation for T_T to define T for all z and ν (or z and s, etc.). Hence in general we have

$$T(z,\nu)=P(z,\nu)+\int_0^\infty d\sigma\int_{-1}^{1}\frac{d\beta}{z+\beta\nu-\sigma}\left[\sum_{m=0}^{M}\nu^m h_m(\sigma,\beta)+\sum_{n=0}^{N}(z+\beta\nu-\sigma)^n\tilde{h}_n(\sigma,\beta)\right] \tag{18}$$

for all z and ν. $T_T(z,\nu)$ is always a boundary value (at $\mathrm{Im}z>0$, $\mathrm{Im}\nu>0$, $\mathrm{Re}\nu>0$ in the s-channel physical region; at $\mathrm{Im}z>0$, $\mathrm{Im}\nu<0$, $\mathrm{Re}\nu<0$ in the u-channel physical region) of an analytic function $T(z,\nu)$ of two complex variables. As we have seen, it may not always be a boundary value of a real analytic function of one complex variable when the other variable is fixed above certain real values. We also note that this analytic continuation is conjugate symmetric in the two complex variables, i.e.,

$$T(z^*,\nu^*)=T^*(z,\nu)\,. \tag{19}$$

This property will also be reflected by the analytic continuations obtained from Feynman graphs. This does not necessarily imply that the physical amplitudes $T(z,\nu_R\pm i\epsilon)$ or $T(z_R\pm i\epsilon,\nu)$ are real analytic functions of one complex variable. Now

$$\begin{aligned}A(z,\nu)&=\int_{-1}^{1}d\beta\int_0^\infty d\sigma\,\epsilon(\tfrac{1}{2}\nu+\beta M^2)\delta(z+\beta\nu-\sigma)H(\sigma,\beta)\\&=\begin{cases}\displaystyle\int_{-1}^{1}d\beta\int_0^\infty d\sigma\,\delta(z+\beta\nu-\sigma)H(\sigma,\beta)=-\frac{1}{\pi}\,\mathrm{Im}T(z,\nu+i\epsilon), & \text{in the } s\text{-channel physical region}\\ \displaystyle\int_{-1}^{1}d\beta\int_0^\infty d\sigma\,\delta(z+\beta\nu-\sigma)H(\sigma,\beta)=-\frac{1}{\pi}\mathrm{Im}T(z,\nu-i\epsilon), & \text{in the } u\text{-channel physical region.}\end{cases}\end{aligned} \tag{20}$$

Thus the absorptive parts $A(z,\nu)$ and $I(z,\nu)$ agree in the various physical regions. They can differ in the unphysical region $\nu^2<4M^2z$, and here $I(z,\nu)$ need not represent the commutator. But in the unphysical region the definition of the Fourier transform of the commutator is arbitrary, since neither the DGS representation nor any general principles indicate any analyticity for these absorptive parts, and so we have no *a priori* criterion to choose one over the other. Thus different representations of the commutator in the unphysical region, which agree on the physical region, will give the same amplitude and the same physics. Since we have chosen a particular representation for the amplitude on the *a priori* basis of analyticity, it is convenient to choose its total imaginary part $I(z,\nu)$ to define the commutator even in the unphysical region. One advantage of such definition is that the analytic continuation of the amplitude into a particular complex domain is unique and so has a unique imaginary part. In the particular case of a real analytic function (only real cuts), the total discontinuity across the real cut gives the imaginary part. For an analytic function with complex cuts (as is needed to define the analytic continuation of the amplitude in the case when the DGS representation indicates a nonvanishing imaginary part across the whole real axis) the imaginary parts in the real region on the physical sheet are related to the discontinuities across the complex cuts[7] also. This will become clear when we discuss Feynman graphs. As an example, we should note the fact that since the DGS representation for T tells us that T is a real analytic function of z for all fixed real ν, we can, therefore, unambiguously define the imaginary part $I(z,\nu)$ as the total discontinuity across the (real) cuts in the z plane for any real z and ν, and we can take this to define the commutator for all real z and ν.

Before we conclude this section we discuss Nakanishi's[4c] method of deriving the DGS representation from the Nambu[2,6a-6c] representation for an arbitrary-order Feynman graph for the virtual forward Compton scattering amplitude, and apply the results to the box graph of Fig. 8(a). In particular, we explicitly demonstrate how to use this representation

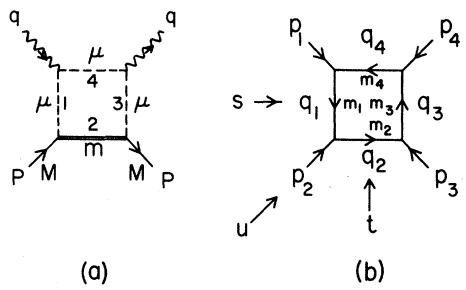

FIG. 8. The direct-channel box diagram: (a) for special masses, (b) for general masses.

to study the "scaling" of the contribution of any Feynman graph to the inelastic structure functions W.

For an arbitrary Feynman graph, with N internal legs and l independent loops, for the VFC amplitude the Nambu representation[2a,6a-6c] is written as

$$T(z,s,M^2)=\lim_{E\to 0+} G(N-2l-1)!\int_0^1\left(\prod_{i=1}^N d\alpha_i\right)\delta\left(\sum_{i=1}^N\alpha_i-1\right)\frac{C(\{\alpha_j\})^{N-2l-2}}{[D(\{\alpha_j\},z,s,M^2)+i\epsilon C]^{N-2l}}\,, \tag{21}$$

where G is a constant. For a u-channel graph the variable s is replaced by u. Applying circuit theory,[2a,6] one can show that the discriminant

$$D(\alpha_1,\ldots,\alpha_N,z,s,M^2)=\xi_s(\alpha_1,\ldots,\alpha_N)s+\xi_z(\alpha_1,\ldots,\alpha_N)z+\xi_u(\alpha_1,\ldots,\alpha_N)u+\xi_M(\alpha_1,\ldots,\alpha_N)M^2-C(\{\alpha_j\})\sum_{j=1}^N\alpha_j m_j^2, \tag{22}$$

while $C(\{\alpha_i\})$ is a sum of products of $\{\alpha_i\}$ and for[3a]

$$0\le\alpha_i\le 1,\quad \xi_\nu(\{\alpha_j\})\ge 0,\quad \nu=s,z,u,M,\quad \{j\}=1,2,\ldots,N,\quad \text{and}\quad C(\{\alpha_i\})\ge 0. \tag{23}$$

Again we define

$$\eta(\{\alpha_i\})=\xi_s(\{\alpha_i\})+\xi_z(\{\alpha_i\})+\xi_u(\{\alpha_i\})\ge 0,$$

$$\phi(\{\alpha_i\})=\frac{\xi_s(\{\alpha_i\})-\xi_u(\{\alpha_i\})}{\xi_s(\{\alpha_i\})+\xi_z(\{\alpha_i\})+\xi_u(\{\alpha_i\})},\quad -1\le\phi(\alpha_i)\le 1 \tag{24}$$

$$\psi(\{\alpha_i\},m_i^2,M^2)=\left(C(\{\alpha_i\})\sum_{j=1}^N\alpha_j m_j^2-[\xi_s(\{\alpha_i\})+\xi_u(\{\alpha_i\})+\xi_M(\{\alpha_i\})]M^2\right)\Big/\eta(\{\alpha_i\}),$$

and use $s=z+\nu+M^2$ and $u=z-\nu+M^2$ to write

$$D=\eta(z+\phi\nu-\psi). \tag{25}$$

To get a representation with a DGS type of denominator, we use the identity

$$1=\int_{-\infty}^{\infty}d\beta\,\delta(\beta-\phi)\int_{-\infty}^{\infty}d\sigma\,\delta(\sigma-\psi) \tag{26}$$

and

$$\int_{-\infty}^{\infty}d\sigma\,\frac{\delta(\sigma-\psi)}{(A-\sigma)^{n+1}}=\frac{(-1)^n}{n!}\int_{-\infty}^{\infty}\frac{d\sigma}{A-\sigma}\,\frac{\partial^n}{\partial\sigma^n}\,\delta(\sigma-\psi),\quad n\ge 1 \tag{27}$$

after n partial integrations.

We use $\delta(\sum\alpha_i-1)$ to extend the α_i integrations to infinity and assume suitable convergence properties so as to be able to interchange the order of the α_i, β, and σ integrations to get

$$\begin{aligned}T(z,s,M^2)&=G(N-2l-1)!\int_{-\infty}^{\infty}d\beta\int_0^{\infty}\left(\prod_{i=1}^N d\alpha_i\right)\frac{C(\{\alpha_j\})^{N-2l-2}}{\eta^{N-2l}}\,\delta\left(\sum_{i=1}^N\alpha_i-1\right)\delta(\beta-\phi)\int_{-\infty}^{\infty}d\sigma\,\frac{\delta(\sigma-\psi)}{(z+\beta\nu-\sigma)^{N-2l}}\\&=G(-1)^{N-2l-1}\int_{-\infty}^{\infty}d\beta\int_{-\infty}^{\infty}\frac{d\sigma}{z+\beta\nu-\sigma}\int_0^{\infty}\left(\prod_{i=1}^N d\alpha_i\right)\frac{C(\{\alpha_j\})^{N-2l-2}}{\eta^{N-2l}}\,\delta\left(\sum_{i=1}^N\alpha_i-1\right)\delta(\beta-\phi)\,\frac{\partial^{N-2l-1}\delta(\sigma-\psi)}{\partial\sigma^{N-2l-1}}\,.\end{aligned} \tag{28}$$

If we define the DGS spectral function

$$H(\sigma,\beta)=G(-1)^{N-2l-1}\int_0^{\infty}\left(\prod_{i=1}^N d\alpha_i\right)\frac{C(\{\alpha_j\})^{N-2l-2}}{\eta^{N-2l}}\,\delta\left(\sum_{i=1}^N\alpha_i-1\right)\delta(\beta-\phi)\,\frac{\partial^{N-2l-1}\delta(\sigma-\psi)}{\partial\sigma^{N-2l-1}}\,, \tag{29}$$

we get the DGS representation

$$T(z,\nu)=\int_{-\infty}^{\infty}d\beta\int_{-\infty}^{\infty}d\sigma\,\frac{H(\sigma,\beta)}{z+\beta\nu-\sigma}\,. \tag{30}$$

To find the support of the spectral function $H(\sigma,\beta)$, we use the δ functions and note that by its definition

$-1\le\phi\le 1$ for $0\le\alpha_i\le 1$,

implying that $H(\sigma,\beta)$ is nonzero only for $0\leq\beta\leq 1$. Similarly $H(\sigma,\beta)$ is nonzero only for $\psi_{\min}\leq\sigma\leq\psi_{\max}$, where $\psi_{\min\,(\max)}$ is the minimum (maximum) value of ψ subject to the constraint that $\phi=\beta$ lie at a fixed given value in the interval $[-1,1]$. Therefore the support of $H(\sigma,\beta)$ is the two-dimensional region

$$\{-1<\beta\leq 1,\ \psi_{\min}\leq\sigma\leq\psi_{\max}\}.$$

To get a feel for the representation, we determine its spectral function for some examples. For poles of the form $T(z,\nu)=C/(z-m^2)$ we get $H(\sigma,\beta)=C\delta(\beta)\delta(\sigma-m^2)$. For poles of the form

$$T(z,\nu)=\frac{1}{s-m^2}\pm\frac{1}{u-m^2} \tag{31}$$

we get

$$H(\sigma,\beta)=[\delta(\beta-1)\pm\delta(\beta+1)]\,\delta(\sigma-m^2+M^2), \tag{32}$$

while

$$H(\sigma,\beta)=\theta(1-\beta^2)\frac{\partial}{\partial\sigma}\,\delta(\sigma-m^2+M^2) \tag{33}$$

gives

$$T(z,\nu)=\frac{2}{(s-m^2)(u-m^2)}. \tag{34}$$

Now we use this method to determine the explicit DGS representation for the box diagram of Fig. 8(a). Here $N=4$, $l=1$,

$$\begin{aligned}\xi_s&=\alpha_2\alpha_4,\\ \xi_z&=\alpha_4(\alpha_1+\alpha_3),\\ \xi_M&=\alpha_2(\alpha_1+\alpha_3),\end{aligned} \tag{35}$$

while

$$\begin{aligned}\xi_u&\equiv 0,\\ \eta&=\alpha_4(\alpha_1+\alpha_2+\alpha_3)=\alpha_4(1-\alpha_4),\\ \phi&=\frac{\alpha_2}{\alpha_1+\alpha_2+\alpha_3}=\frac{\alpha_2}{1-\alpha_4},\quad 0\leq\frac{\alpha_2}{1-\alpha_4}\leq 1\\ \psi&=\frac{1}{\alpha_4(1-\alpha_4)}\left(\sum_{i=1}^{4}\alpha_i m_i{}^2-\alpha_2(1-\alpha_2)M^2\right)=\frac{(1-\alpha_2)\mu^2+\alpha_2{}^2M^2}{\alpha_4(1-\alpha_4)},\end{aligned} \tag{36}$$

$C=\alpha_1+\alpha_2+\alpha_3+\alpha_4=1$ because of the δ function.

So the DGS representation is

$$B(z,\nu)=\int_0^1 d\beta\int_{-\infty}^{\infty}d\sigma\frac{H(\sigma,\beta)}{z+\beta\nu-\sigma}, \tag{37}$$

where

$$H(\sigma,\beta)=-G\int_0^{\infty}\left(\prod_{i=1}^{4}d\alpha_i\right)\delta\left(\sum_{i=1}^{4}\alpha_i-1\right)\frac{\delta(\beta-\phi)}{\eta^2}\frac{\partial}{\partial\sigma}\,\delta(\sigma-\psi). \tag{38}$$

Performing the α_1 and α_3 integrations using one δ function gives

$$H(\sigma,\beta)=-G\int_0^1\int_0^1 d\alpha_2 d\alpha_4\,\frac{(1-\alpha_4-\alpha_2)\theta(1-\alpha_4-\alpha_2)}{\alpha_4{}^2(1-\alpha_4)^2}\,\delta\left(\beta-\frac{\alpha_2}{1-\alpha_4}\right)\frac{\partial}{\partial\sigma}\,\delta(\sigma-\psi). \tag{39}$$

Put $1-\alpha_4=\alpha$ and $\alpha_2/\alpha=y$ and use the θ functions to get

$$H(\sigma,\beta)=-G\int_0^1\frac{d\alpha}{(1-\alpha)^2}\int_0^1 dy(1-y)\delta(y-\beta)\frac{\partial}{\partial\sigma}\,\delta\left(\sigma-\frac{(1-\alpha y)\mu^2+\alpha^2y^2M^2}{\alpha(1-\alpha)}\right). \tag{40}$$

Use a δ function to do the y integration to get

$$H(\sigma,\beta)=-G[\theta(\beta)-\theta(\beta-1)](1-\beta)\int_0^1\frac{d\alpha}{(1-\alpha)^2}\frac{\partial}{\partial\sigma}\delta\left(\sigma-\frac{(1-\beta\alpha)\mu^2+\beta^2\alpha^2M^2}{\alpha(1-\alpha)}\right). \tag{41}$$

Assuming we can interchange the order of integration and differentiation, we get

$$H(\sigma,\beta)=-G[\theta(\beta)-\theta(\beta-1)](1-\beta)\frac{\partial}{\partial\sigma}\int_0^1\frac{d\alpha}{(1-\alpha)^2}\delta\left(\sigma-\frac{\beta^2\alpha^2M^2-\beta\alpha\mu^2+\mu^2}{\alpha(1-\alpha)}\right). \tag{42}$$

Call

$$I(\sigma)\equiv\int_0^1\frac{d\alpha}{(1-\alpha)^2}\delta\left(\sigma-\frac{\beta^2\alpha^2M^2-\beta\alpha\mu^2+\mu^2}{\alpha(1-\alpha)}\right)=\int_{-\infty}^{\infty}d\alpha\frac{\theta(\alpha)-\theta(\alpha-1)}{(1-\alpha)^2}\delta(g(\alpha)). \tag{43}$$

We define

$$g(\alpha)=\sigma-\frac{\beta^2\alpha^2M^2-\beta\alpha\mu^2+\mu^2}{\alpha(1-\alpha)}\equiv(\sigma+\beta^2M^2)\frac{(\alpha-\alpha_+)(\alpha-\alpha_-)}{\alpha(\alpha-1)}, \tag{44}$$

where

$$\alpha_\pm(\sigma,\beta)=\frac{(\sigma+\beta\mu^2)\pm[\sigma^2+2\mu^2(\beta-2)\sigma-\beta^2\mu^2(4M^2-\mu^2)]^{1/2}}{2(\sigma+\beta^2M^2)}, \tag{45}$$

$$g'(\alpha)=(\sigma+\beta^2M^2)\left[\frac{(2\alpha-\alpha_+-\alpha_-)}{\alpha(\alpha-1)}-\frac{(\alpha-\alpha_+(\alpha-\alpha_-)(2\alpha-1)}{\alpha^2(\alpha-1)^2}\right].$$

Doing the α integration, we get

$$I(\sigma)=\frac{\theta(\alpha_+)-\theta(\alpha_+-1)}{|g'(\alpha_+)|(1-\alpha_+)^2}+\frac{\theta(\alpha_-)-\theta(\alpha_--1)}{|g'(\alpha_+)|(1-\alpha_-)^2}, \tag{46}$$

where the θ functions are interpreted to vanish if $\alpha_\pm$ are complex.

To see the use of having the explicit form of the DGS function, we calculate

$\lim_{\nu\to\infty}\nu\mathrm{Im}B(z,\nu)$ for $z<0$ and $x=\frac{z}{\nu}$ fixed.

We expect from our calculation in Sec. IV that for $z<0$

$$\lim_{\nu\to\infty,\,x\text{ fixed}}\nu\mathrm{Im}B(z,\nu)=\lim_{\nu\to\infty}\frac{\nu}{2i}\,\mathrm{disc}_sB(z,\nu)$$

$$=\mathrm{const}\frac{(1+x)[\theta(-x)-\theta(-x-1)]}{M^2x^2+\mu^2x+\mu^2}. \tag{47}$$

To calculate this from the DGS representation, we note that

$$\mathrm{Im}B(z,\nu)=-\pi\int_{-\infty}^{\infty}d\sigma\int_{-\infty}^{\infty}d\beta\,H(\sigma,\beta)\delta(z+\beta\nu-\sigma). \tag{48}$$

Doing the β integration and using the support of $H(\sigma,\beta)$, we get

$$\lim_{\nu\to\infty}\frac{\nu\mathrm{Im}B(z,\nu)}{-\pi}=\lim_{\nu\to\infty}\int_{-\infty}^{\infty}d\sigma\left[\theta\left(\frac{\sigma}{\nu}-x\right)-\theta\left(\frac{\sigma}{\nu}-x-1\right)\right]H\left(\sigma,\frac{\sigma}{\nu}-x\right). \tag{49}$$

Assuming we can interchange the order of integration and the limit, and assuming that the limit of a product of distributions is the product of their limits, we get

$$\lim_{\nu\to\infty}\frac{\nu\mathrm{Im}B(z,\nu)}{-\pi}=\int_{-\infty}^{\infty}d\sigma[\,\theta(-x)-\theta(-x-1)]\lim_{\nu\to\infty}H\left(\sigma,\frac{\sigma}{\nu}-x\right). \tag{50}$$

Now one may be tempted to claim without further assumption[1f] that

$$\lim_{\nu\to\infty}H\left(\sigma,\frac{\sigma}{\nu}-x\right)=H(\sigma,-x). \tag{51}$$

But it is important to note that this could be false since $H(\sigma,\beta)$ is a distribution which is defined as a limit of a sequence. So, to use the above result, we must assume that we can interchange the limit $\nu\to\infty$ and the limit of the sequence defining the distribution. Assuming this, we get

$$\lim_{\nu\to\infty} \nu \mathrm{Im}B(z,\nu) = -\pi\int_{-\infty}^{\infty} d\sigma[\theta(-x)-\theta(-x-1)]H(\sigma,-x). \tag{52}$$

Substituting the $H(\sigma,-x)$ obtained for the box graph, we get

$$\lim_{\nu\to\infty} \nu \mathrm{Im}B(z,\nu) = \pi G[\theta(-x)-\theta(-x-1)](1+x)\int_{-\infty}^{\infty} d\sigma \frac{\partial}{\partial\sigma} I(\sigma)$$

$$= \pi G[\theta(-x)-\theta(-x-1)](1+x)[I(+\infty)-I(-\infty)]. \tag{53}$$

Now $I(-\infty)=0$, since the δ function cannot be satisfied for $0 \leq \alpha \leq 1$.

To calculate $I(+\infty)$ we note that

$$\alpha_{\pm}(\sigma,\beta) \sim \frac{\sigma - x\mu^2 \pm [\sigma - x\mu^2 - 2\mu^2 + O(1/\sigma)]}{2(\sigma + x^2M^2)}, \quad \sigma \to +\infty \tag{54}$$

so that

$$\alpha_+ \sim \frac{\sigma - x\mu^2 - \mu^2}{\sigma + x^2M^2} + O(1/\sigma^2),$$

$$\alpha_- \sim \frac{\mu^2}{\sigma + x^2M^2} + O(1/\sigma^2). \tag{55}$$

Then

$$I(\sigma) = \frac{[\theta(\alpha_+)-\theta(\alpha_+-1)]|\alpha_+|}{(\sigma+x^2M^2)(1-\alpha_+)|\alpha_+-\alpha_-|} + \frac{[\theta(\alpha_-)-\theta(\alpha_--1)]|\alpha_-|}{(\sigma+x^2M^2)(1-\alpha_-)|\alpha_+-\alpha_-|},$$

$$\sim \frac{1}{M^2x^2+\mu^2x+\mu^2}, \quad \sigma\to\infty. \tag{56}$$

Therefore

$$\lim_{\nu\to\infty} \nu \mathrm{Im}B(z,\nu) = \pi G \frac{[\theta(-x)-\theta(-x-1)](1+x)}{M^2x^2+\mu^2x+\mu^2}, \tag{57}$$

which agrees with the result obtained by direct laborious calculation of the discontinuities. This demonstrates the utility of having the explicit form of the DGS spectral function of any Feynman graph for studying the "scaling" of its contribution to the inelastic structure functions.[1] For this purpose one should also include spin, which has the effect of altering the function $C(\alpha)$ and adding external momentum-dependent factors in the numerator,[9a] but the technique for obtaining the DGS representation remains unchanged. We should also be careful about the infrared and ultraviolet divergences.[2a,6]

The above result also shows that the complex anomalous poles in the discontinuities indicated by our general analysis are also shown by the DGS representation when the explicit form of the spectral function is calculable. On the other hand, in spite of being equivalent to the Nambu representation, the DGS representation in its general form is very inconvenient to continue into the unphysical region due to the apparently singular nature of its spectral function. That is why, for example, the resonance poles on the second sheet are hard to represent in the DGS form.

IV. RESULTS FROM PERTURBATION THEORY

To understand what happens to the analyticity of the amplitude T when its absorptive part is nonzero on the entire real axis, we study the analytic structure of the Feynman integral represented by the box diagram of Fig. 8. This is the simplest graph exhibiting a nontrivial cut structure. Since spin is unimportant in our discussions, we take all particles to be scalars and the internal masses in Fig. 8(a) are chosen to reflect the $t=0$ symmetry of the graph. The generalized Mandelstam representations in the complex s and t planes for this diagram have been extensively studied by several authors in cases when one fixed external mass is unstable, or when a pair of equal external masses are unstable[12] (like the off-mass-shell forward Compton amplitude). Unfortunately these representations do not display the analytic structure at $t=0$ in the complex mass plane and so we have to start afresh.

A. The Bjorken-Landau-Cutkosky Method

We use the Bjorken-Landau-Cutkosky method[6] for analyzing the singularities of integrals. The details of this method are very clearly explained

in the first two chapters of the book ELOP[2a,2c] and hence omitted here. We simply outline the method to establish notation and terminology.

It is well known[2,6-10] that the singularities (in the space of complex external variables) of the analytic continuations of integrals, like the Feynman integral, arise when the singularities of their integrands, moving as functions of the external variables, either lie at an "end point" of integration or two (or more) of them "pinch" the integration hypercontour between them so that it cannot be distorted without crossing one of them. This is because, if such situations did not arise in all the integrations, we could use the Cauchy's theorem to deform the contour away from the singularities of the integrand to define an analytic function. This analytic function would analytically continue the Feynman integral, since the distortion of the hypercontour is equivalent to moving the external variables away from the singular point of the Feynman integral. The original integral is then a boundary value of this analytic continuation.

Such analysis applied to the Feynman integral shows that all its singularities are given by a set of equations first obtained by Bjorken[2e] and Landau,[8a] which require that

(1) for each internal line i of the Feynman graph either $q_i^2 = m_i^2$ or $\alpha_i = 0$, where the $\{\alpha_i\}$'s are the Feynman parameters; and

(2) for each loop j of the internal momenta $\sum_{(j)} \alpha_i q_i = 0$, where $\sum_{(j)}$ denotes summation along the jth loop of the internal momenta.

For a given Feynman graph, the leading singularity corresponds to all $\alpha_i > 0$ (no $\alpha_i = 0$). The q-order lower singularities correspond to the q of the $\alpha_i = 0$ and the remaining $\alpha_j > 0$, and are shared by the reduced or contracted graphs in which the q lines with $\alpha_i = 0$ have been shrunk to a point. The location of the complete set of singularities is given by the leading singularities of the original graph together with all its reduced graphs.

The physical boundary is determined by the Feynman prescription of giving all the internal masses an infinitesimal negative imaginary part ($m_i^2 \to m_i^2 - i\epsilon$).

The solutions of the Landau equations with all $\alpha_i \geq 0$ correspond to singularities of the Feynman integral with undistorted hypercontour. In the presence of several branch points the definition of the various sheets of the complex domain depends on the choice of the cuts attached to these branch points. We define the "physical sheet" as the sheet of the normal threshold cuts which carries the physical boundary. Normal thresholds, in general, are the lowest-order singularities of a given Feynman integral and they lie in the physical region.[6p] We collectively call the higher-order singularities the anomalous singularities. The anomalous singularities found on the physical sheet are the ones which move onto it during the process of analytic continuation. Among the various possible methods[2a,2c,6d] for the anomalous singularities to come on the physical sheet the most common is the mechanism of "critical intersections," and much less common ones are the mechanisms of "cusps" and "acnodes."[13] The type of graphs or the conditions under which cusps and acnodes have been found do not seem to occur for the scattering amplitude at $t = 0$, since its dual diagram is topologically similar to that of a vertex. We therefore assume their absence and restrict our discussion to the mechanism of critical intersection, which corresponds to a pinch moving onto the undistorted hypercontour past an end point. With this mechanism the only anomalous singularities found on the physical sheet are the ones which climb onto it through the normal threshold cuts, or through the cuts attached to the (lower-order) branch points which have previously come onto the physical sheet through the normal thresholds. The required condition for one Landau singularity to change sheets by moving through the cut attached to another Landau singularity is that their Landau curves "touch effectively" (or intersect critically). For two Landau curves to "touch effectively" they must touch and at the point of touch have identical values for all the Feynman parameters α_i. It is easy to prove that the intersection (if it occurs) of any Landau curve with any one-order-lower Landau curve is necessarily effective. But as we will see (in Figs. 13 and 14), once an effective touch is established one must check that the singularity does in fact cross the lower-order cut. This requires that the point of touching be a turning point of the higher-order Landau curve relative to the lower-order Landau curve.

These singularities can be poles or branch points depending on various factors like the dimensionality of space-time, the redundancy in the Landau equation for a given graph, spin, form factors, and nature of the couplings. The poles and the branch points can be distinguished in practice by one of two methods. Either we calculate the discontinuity (using the Cutkosky formula[10]) across the given singularity and see if it is finite or a δ function (a δ-function discontinuity indicates a pole) or, alternatively, we calculate the discontinuity across a lower-order singularity and in it see explicitly the presence of the pole due to the given higher-order singularity.[7c]

The singularities obtained from the solution of the Landau equations fall into three main classes which are conveniently categorized in terms of the Nambu representation (see Sec. III). These are

the Landau singularities ($D=0$, $C\neq 0$), or the mixed or pure non-Landau (or second type) singularities ($D=0$, $C=0$). The Landau singularities[6,8] correspond to pinches and end-point singularities when all the components of the loop momenta are finite. The second-type[9,7c] singularities correspond to a wide class of special solutions of the Landau equations, which correspond to pinches when either all (pure) or some (mixed) components of the loop momenta are infinite. In the present paper we shall mainly concern ourselves with the Landau singularities, since very little is known about the Riemann-sheet properties of the second-type singularities. The presence or absence of the second-type singularities depends on the dimensionality of space-time, but can also be affected by spin and derivative couplings. It has been expected[9a] that the pure second-type singularities for a scattering graph always stay away from the physical sheet, and their position can be found in terms of the momenta p_i of the external legs only. They are located at the edges of the physical region (s or u $=0, 4M^2$), where

(i) $\det(p_i\cdot p_j)=0$

($i,j=1,2,\ldots,E=$ number of external legs) and

(ii) $p_j\cdot\sum_{i=1}^{E}p_i=0$ and $\left(\sum_{i=1}^{E}p_i\right)^2=0$.

The situation regarding the mixed second-type singularities[7c] is not so clear. They orginate on the unphysical sheet, since they need $C(\alpha)$ for a subgraph to vanish [and $C(\alpha)$ being a sum of products of α's cannot vanish for $\alpha>0$]. But it is not known in general whether they come onto the physical sheet through a cut on the physical sheet, when an analytic continuation is performed. The necessary conditions for this to occur are that the second-type singularity curve either has an "effective intersection" with some other curve that is itself singular on the physical sheet or that the curve contains acnodes or cusps.[2a,13]

The reason that the second-type singularities can be important even if they stay on the second sheet is that the discontinuities in general display the singularities of both the physical and the second sheet, and in fact that is how the second-type singularities were discovered. It is the lack of knowledge of the second-sheet singularities that restricts us to discussing only the single-variable analyticity of the discontinuities, which only involves the ordinary and virtual[2c] anomalous singularities on the physical sheet of the amplitude.

B. The Box Diagram

Consider the general box diagram of Fig. 8. Using the Feynman parameters and doing the loop integration, we obtain the "Nambu representation" for this graph:

$$B(p_1,p_2,p_3,p_4)=\text{const}\int_0^1\int_0^1\int_0^1\int_0^1\frac{d\alpha_1 d\alpha_2 d\alpha_3 d\alpha_4\,\delta(\alpha_1+\alpha_2+\alpha_3+\alpha_4-1)C^0}{D^2}\,, \tag{58}$$

where

$$D=\alpha_2\alpha_4 s+\alpha_1\alpha_3 t+\alpha_4\alpha_1 p_1^{\,2}+\alpha_1\alpha_2 p_2^{\,2}+\alpha_2\alpha_3 p_3^{\,2}+\alpha_3\alpha_4 p_4^{\,2}-\left(\sum_{n=1}^{4}\alpha_i\right)\left(\sum\alpha_i m_i^{\,2}\right),$$

$$C=\alpha_1+\alpha_2+\alpha_3+\alpha_4\,.$$

If we define the variables

$$y_{ij}=-\frac{q_i\cdot q_j}{m_i m_j}\equiv y_{ji},\quad y_{ii}=-1 \tag{60}$$

then for the single-loop box graph the equation of the surface of the Landau singularities is given by

$$\det(y_{i,j})=0\,, \tag{61}$$

and the vanishing of the various minors of $\det(y_{i,j})$ corresponds to the lower-order singularities due to the reduced graphs shown in Fig. 9. For future reference we list the equations for the various Landau surfaces in the two-dimensional complex space of external variables, starting with the leading singularity.

(1) The "box singularity" which corresponds to Fig. 8 or Fig. 9(a): In this case we need ($m_1=m_3=\mu$)

$$\det(y_{i,j})=-\frac{t}{\mu^2}\mathfrak{D}_3(t)\,,$$

where

$$\mathfrak{D}_3(t)\equiv\begin{vmatrix} -1 & \dfrac{M^2-\mu^2-m_2^{\,2}}{2\mu m_2} & \dfrac{s-m_2^{\,2}-m_4^{\,2}}{2m_2m_4}\\ \dfrac{M-\mu^2-m_2^{\,2}}{2\mu m_2} & -1+\dfrac{t}{4\mu^2} & \dfrac{z^2-\mu^2-m_4^{\,2}}{2\mu m_4}\\ \dfrac{s-m_2^{\,2}-m_4^{\,2}}{2m_2m_4} & \dfrac{z-\mu^2-m_4^{\,2}}{2\mu m_4} & -1\end{vmatrix}. \tag{63}$$

At fixed $t=0$ the box singularity is given by the equation

$$\mathfrak{D}_3^{(0)}=0\ \text{ and }\ m_1=m_3\,, \tag{64}$$

which is identical to the equation of the physical-sheet "triangle singularity" corresponding to the

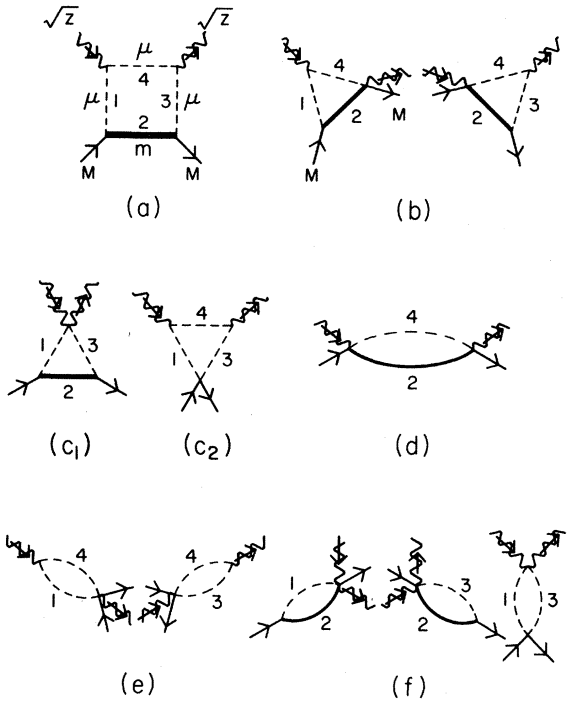

FIG. 9. The reduced graphs for the leading and lower-order Landau singularities for the direct s-channel box diagram.

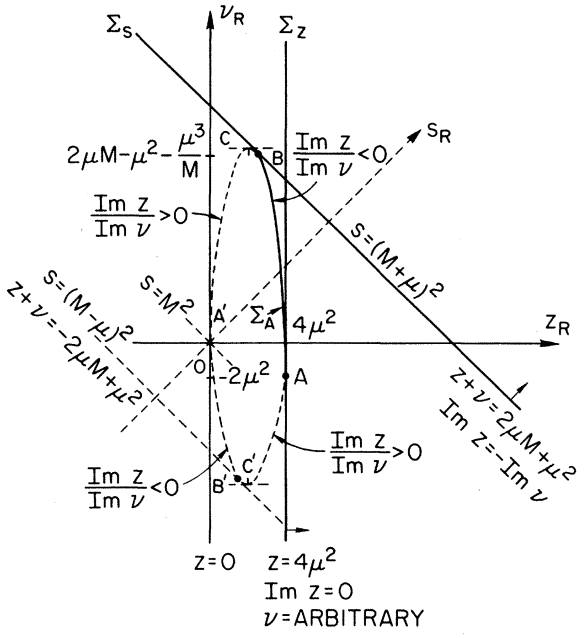

FIG. 10. The Landau curves in the real (z,ν) plane for the case $m=M$. The equation of the ellipse $ABA'B'$ is $M^2z^2+\mu^2z\nu+\mu^2\nu^2-\mu^2(4M^2-\mu^2)z=0$, and the coordinates of the points of tangency are $A=(4\mu^2,-2\mu^2)$, $B=(2\mu^2+\mu^3/M,\ 2\mu M-\mu^2-\mu^3/M)$, $A'=(0,0)$, $B'=(2\mu^2-\mu^3/M,\ 2\mu M-\mu^2+\mu^3/M)$.

reduced graph of Fig. 9(b). For $t\neq 0$ one defines a complex cut joining [see Ref. 14, especially Ref. 14c] the box branch point ($1/\sqrt{\xi}$ type) and the triangle branch point ($\ln\xi$ type). But in the $t=0$ case these two points coincide giving a collapsed cut which, as we will see later, acts like a simple pole[14c,14d] and could have a dominating effect in the appropriate regions.

(2) The "triangle singularities" corresponding to Figs. 9(b), 9(c_1), and 9(c_2): Corresponding to Fig. 9(b) we have the anomalous threshold surface Σ_A whose equation $\mathfrak{D}_3^{(0)}=0$ can be written as

$$M^2z^2+(M^2-m^2+\mu^2)z\nu+\mu^2\nu^2+\triangle z=0\,, \tag{65}$$

where

$$\triangle\equiv[M^2-(m+\mu)^2][M^2-(m-\mu)^2]\,. \tag{66}$$

The shape of its conic section with the real plane (z_R,ν_R) is determined by the discriminant, which turns out to be $\triangle$. It is an ellipse, parabola, or hyperbola depending on whether $\triangle<0$, $=0$, or >0. It is easy to see by an analysis similar to that for the triangle graph in ELOP, that the condition for this triangle singularity to be on the physical sheet of the VFC amplitude is $\triangle<0$, i.e., an elliptic curve with the normal threshold surfaces as tangent planes. This then restricts m to be $|M-\mu|<m<M+\mu$. Figures 10, 11, and 12 show the real section of this surface Σ_A under various conditions.

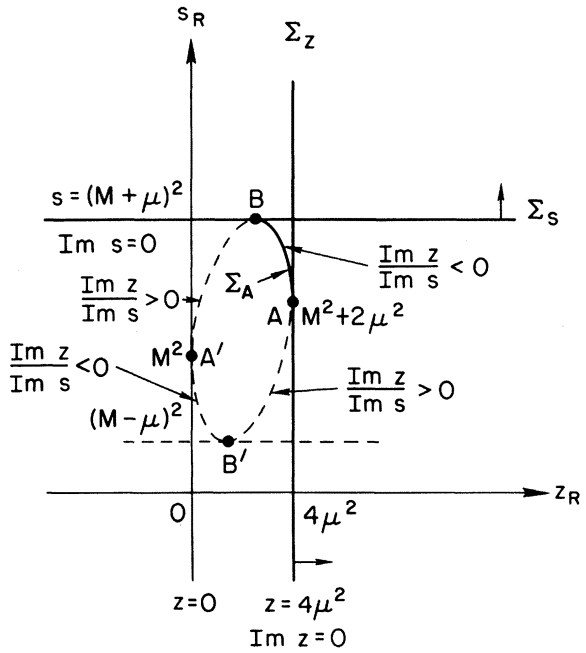

FIG. 11. The Landau curves in the real (z,s) plane for the case $m=M$. The equation of the ellipse $ABA'B'$ is $M^2z^2+\mu^2(\mu^2-3M^2-s)z+\mu^2(s-M^2)^2=0$, and the coordinates of the points of tangency are $A=(4\mu^2,\ M^2+2\mu^2)$, $B=(2\mu^2+\mu^3/M,\ (M+\mu)^2)$, $A'=(0,M^2)$, $B'=(2\mu^2+\mu^3/M,\ (M-\mu)^2)$.

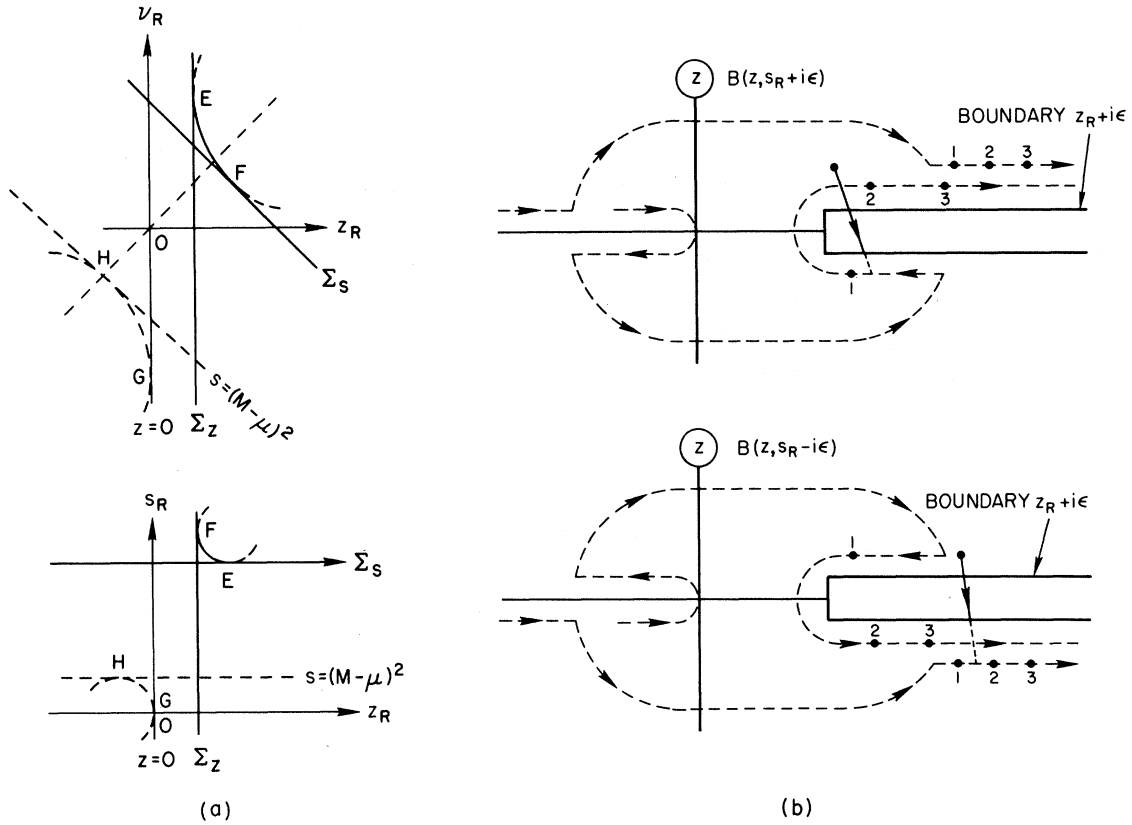

FIG. 12. (a) The real section of the Landau surfaces for $m \geq M + \mu$ when we get an hyperbola. (b) Virtual singularities close to the physical boundary of $\mathrm{disc}_s B(z, s_R)$.

To obtain the solution of the above equation for general masses we recommend that the reader use the method of dual diagrams.[8] To draw the complex parts of Σ_A requires another two dimensions. To get over this difficulty we use the search-line method. We imagine a plane in the complex (z, ν) space. This is

$$\nu = \psi z + \eta, \quad \psi, \eta \text{ real}$$
$$\mathrm{Im}\nu = \psi \, \mathrm{Im} z . \tag{67}$$

It intersects the real conic section of the quadratic surface Σ_A in the real (z_R, ν_R) planes at two unique points. If its slope is kept fixed and the intercept η increased, the line moves upwards in a direction perpendicular to itself and the two points of intersection form a pair of continuous curves on the Landau surface. Eventually these two real intersections with the search line coalesce, and after that they are no longer real and become a pair of complex-conjugate points, with the imaginary parts of their coordinates related by the above equation. Nothing is missed since every complex point lies on one and only one search line.

Using such search lines, we discover that attached to the positive-gradient arcs of the real conic sections are two parts of a complex surface with $\mathrm{Im}\nu/\mathrm{Im}z = \psi > 0$, while attached to the negative-gradient real arcs are two parts of a complex surface with $\mathrm{Im}\nu/\mathrm{Im}z = \psi < 0$. Along horizontal tangents $\psi = 0$, $\mathrm{Im}\nu = 0$, and $\mathrm{Im}z$ is arbitrary, while along the vertical tangent $\psi = \infty$, $\mathrm{Im}\nu =$ arbitrary, and $\mathrm{Im}z = 0$.

In using this description of the Landau surface to perform an analytic continuation it is frequently important to distinguish the directions along which we approach the real section. For this purpose we define the following limits[2c] onto the real section. When we approach the real domain along $\mathrm{Im}s/\mathrm{Im}z > 0$, we call it the "corresponding half-plane limit," and when we approach along $\mathrm{Im}s/\mathrm{Im}z < 0$ we call it the "opposite half-plane limit." Furthermore, the limit onto the real section of the Landau surface that is defined by giving z and s (or z and ν) small imaginary parts whose relative sign is the same as that which they take on the attached complex Landau surface (i.e., the same as the sign of the slope of the search line) will be called the "appropriate limit." When their relative sign is opposite to that taken on the attached

complex Landau surface we call it the "inappropriate limit." It is easy to see that these limits are different if and only if the sections of the real axes being approached in both variables lie in a cut, i.e., the real section lies in a crossed cut.

If the complex Landau surface is not singular on the physical sheet, then the appropriate limit cannot be singular. If the inappropriate limit is singular, then the singularity is found just past the real boundary of the physical sheet approached by going through the real cut [Fig. 12(b)]. This is quite like the location of the resonance poles at $q^2 = m^2 - im\Gamma$ on the second sheet. Such arcs of real singularities [Fig. 12(a)], which are singular in the inappropriate limit (and hence lie in the region of crossed cuts), are called virtual singularities. These virtual singularities are present in the non-Euclidean region $[\lambda(z, s, M^2) > 0]$ on the real axis (when $\epsilon \to 0$) which lies inside the crossed normal threshold cuts. Their presence is, therefore, not important for the discussion of the domain of analyticity on the physical sheet of the amplitude, though they are near its physical boundary (which lies above or below the cut). On the other hand, their importance for the study of the discontinuities is seen by the fact that in the limit $\epsilon \to 0+$,

$$\mathrm{disc}_s T(z_R + i\epsilon', s_R) \equiv T(z_R + i\epsilon', s_R + i\epsilon) - T(z_R + i\epsilon', s_R - i\epsilon). \quad (68)$$

So we are simultaneously taking the corresponding and opposite half-plane limits of the amplitude T, and therefore $\mathrm{disc}_s T$ will carry both the ordinary (appropriate limit) and virtual (inappropriate limit) anomalous singularities of T.

To find which segments of this four (real) dimensional surface Σ_A are singular on the physical sheet, we use the fact that the Feynman parameters α vary continuously on this surface, so knowing the α's at their effective intersections with the lower-order singularity (the normal threshold tangents), we can deduce the α's on the whole real conic section of Σ_A. In particular, the real segment (solid lines in Figs. 10, 11, and 12) with all $\alpha \geq 0$ is singular on the physical sheet. The complex segment occurs on the analytic continuation by distorting the hypercontour when the α's are complex.

At $t = 0$ the singularities corresponding to the reduced graphs in Figs. 9(c_2) and 9(c_1) are found to coincide with the normal z threshold [Fig. 9(e)] and the normal M^2 threshold [Fig. 9(f)], respectively.

(3) The s-channel normal threshold corresponds to Fig. 9(d), and gives the plane

$$s - M^2 = z + \nu \geq 2\mu M + \mu^2$$

with

$$\mathrm{Im}s = 0, \quad \mathrm{Im}z = -\mathrm{Im}\nu. \quad (69)$$

(4) The z-channel normal threshold corresponds to Figs. 9(c_2) and 9(e) giving the plane

$$z \geq 4\mu^2, \quad \mathrm{Im}z = 0, \quad \nu \text{ arbitrary}. \quad (70)$$

This completes the description of the whole Landau surface of B.

To establish the analytic continuation of B in two complex variables, we just have to show that we can start from the physical boundary and find a singularity-free path to continue the Feynman integral into the complex unphysical domain, making suitable detours when we hit its singularities. To discover the physical boundary we use the Feynman prescription to find

$$\mathrm{Im}D = (\alpha_2\alpha_4 + \alpha_4\alpha_1 + \alpha_4\alpha_3)\mathrm{Im}z + (\alpha_2\alpha_4)\mathrm{Im}\nu + (\alpha_2 \textstyle\sum \alpha_i)\epsilon, \quad \epsilon \to 0+. \quad (71)$$

Therefore the physical boundary of a Feynman integral with real internal masses is

$$\mathrm{Im}z > 0, \quad \mathrm{Im}\nu > 0. \quad (72)$$

The two-variable analyticity is then easily established using techniques explained in ELOP. This continuation is conjugate symmetric, i.e., $B(z, \nu) = B^*(z^*, \nu^*)$. To see this we just have to note that the properties of all the complex segments of the Landau surface are invariant under complex conjugation. Therefore if we start at some real point (z_R, ν_R) and continue to some point (z, ν), the distortion of the α hypercontour forced on us, if any, when we meet singularities will just be the complex conjugate of that forced on us if we had continued by a complex-conjugate path to the complex-conjugate point (z^*, ν^*). Thus the value of B obtained at (z^*, ν^*) will just be the complex conjugate of that obtained at (z, ν).

To establish the analyticity in one complex variable keeping the other fixed in the physical region, we have to study the singularities on a particular search line $z = z_R + i\epsilon$ or $\nu = \nu_R + i\epsilon$. In such cases the Landau curves shown in Figs. 10 and 11 give physical-sheet singularities, while the Landau curves of Fig. 12 do not contribute since they are singular in only the inappropriate limit on the real (z, ν) plane.[2c,6d,6k] Therefore from now on we will not consider them any more, but remember that these virtual singularities occur in the discontinuity, since the whole of the real arc in Fig. 12(a), on which the points E and F lie, is singular in the inappropriate limit. These singularities are nonsingular in the appropriate limit because during the process of analytic continuation they never cross a cut to come onto the sheet chosen as the physical sheet, as shown in Fig. 12(b).

If we consider $B(z, \nu_R + i\epsilon)$ as an analytic function

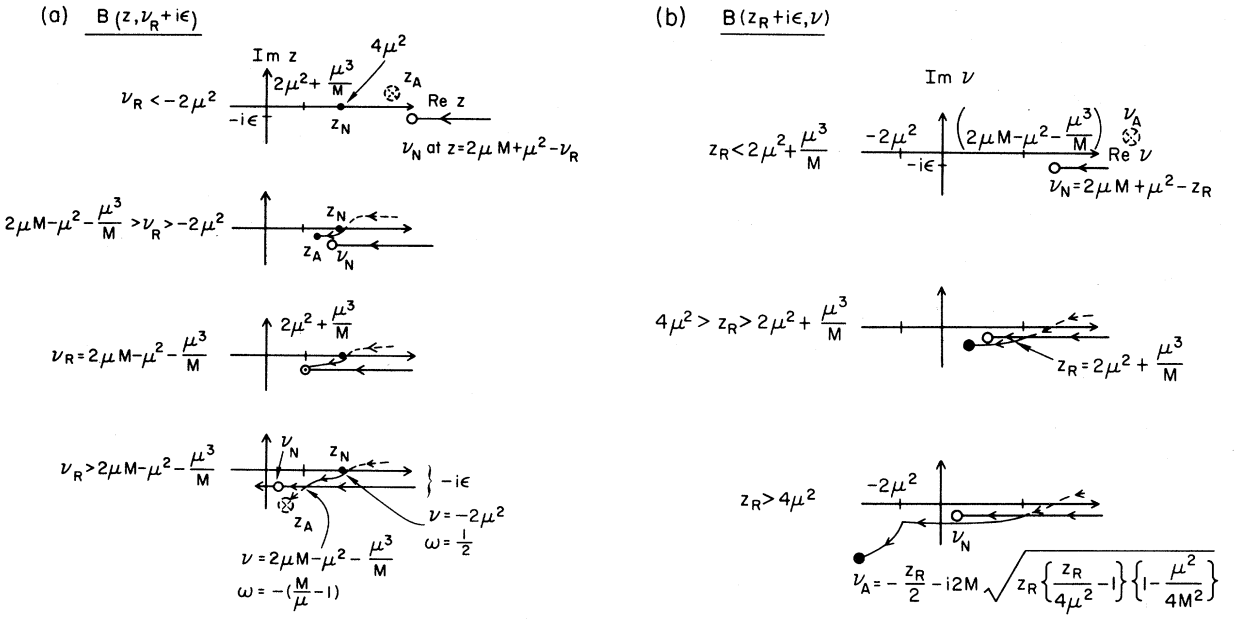

FIG. 13. (a) The single-variable analyticity of $B(z, \nu_R + i\epsilon)$ in the z plane. (b) The single-variable analyticity of $B(z_R + i\epsilon, \nu)$ in the ν plane.

of z, Fig. 13(a) shows the location of various branch points for various values of ν_R. The solid lines indicate the motion of these branch points on the physical sheet, while the dashed lines indicate their motion on the unphysical sheets. We see that Σ_z gives a fixed branch point z_N on the real axis at $z = 4\mu^2$. Σ_s gives a branch point ν_N of $z = 2\mu M + \mu^2 - \nu_R$ which moves just below the real axis. The anomalous branch point A corresponding to the triangle singularity Σ_A is on the unphysical sheet when $\nu_R < -2\mu^2$. As ν_R is increased, A crosses over into the physical sheet through the cut attached to z_N, and when ν_R increases through $\nu_R = 2\mu M - \mu^2 - \mu^3/M$, A again crosses over into the unphysical sheet through the cut attached to the moving branch point ν_N, which leads A beyond this point. So ultimately for large ν_R we are left with the two branch points ν_N and z_N. In the limit $\epsilon \to 0+$, ν_N lies on the real axis. $B(z, \nu_R + i\epsilon)$ therefore has only real cuts attached to the branch points z_N and ν_N, and is therefore a real analytic function for all fixed ν_R.

When we consider $B(z_R + i\epsilon, \nu)$ as an analytic function of ν, Fig. 13(b) shows the location of various branch points for various values of z_R. For $z_R < 2\mu^2 + \mu^3/M$ the branch point ν_N due to Σ_s lies just below the real axis on the physical sheet, while the branch point A due to Σ_A lies on the unphysical sheet. As we increase z_R through $2\mu^2 + \mu^3/M$, the branch point A moves below the real axis and then crosses over onto the physical sheet through the cut attached to the ν_N branch point. As z_R is increased more, the two branch points move infinitesimally below the real axis (A below ν_N) till we reach $z_R = 4\mu^2$. Beyond this value of z_R, the branch point moves to finite distance below the real axis, and since it does not cross any cuts in this process it stays on the physical sheet. This corresponds to the complex segment of Σ_A attached to

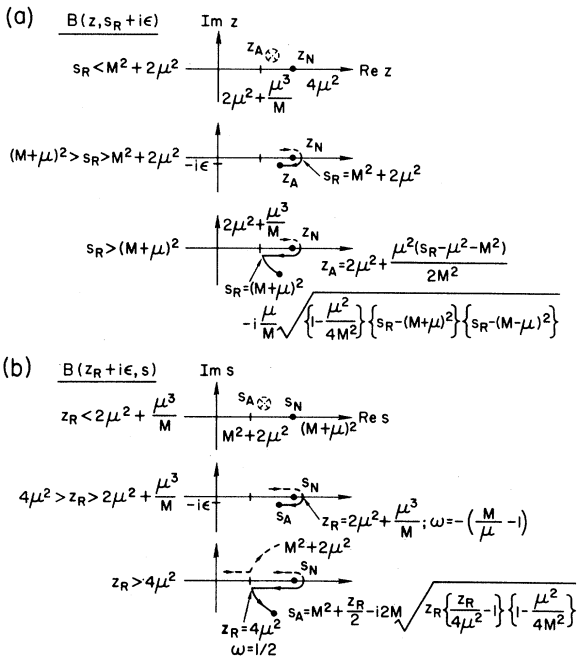

FIG. 14. (a) The single-variable analyticity of $B(z, s_R + i\epsilon)$ in the z plane. (b) The single-variable analyticity of $B(z_R + i\epsilon, s)$ in the s plane.

AB. Thus for $z_R > 4\mu^2$, in the limit $\epsilon \to 0+$ we get a real branch point ν_N and a complex branch point A at ν_A, and $B(z_R + i\epsilon, \nu)$ is no longer a real analytic function of ν. This is consistent with what we expected from our discussion of the DGS representation and also shows that the reason why the DGS representation indicates a nonreal function of ν for $z_R > \mu^2$ (lower bound to $4\mu^2$) is that the analytic continuation acquires complex branch points. At this point we should note the importance of keeping ϵ nonzero and determining the magnitude of the imaginary parts of the various branch points (using search lines). If in the above discussion A were above ν_N, then as we would go through $z_R = 4\mu^2$, A would move down and cross over onto the unphysical sheet through the cut attached to A. It is because A is below ν_N that it remains on the physical sheet as a complex branch point.

We can similarly discuss the analytic structure of B as a function of one variable while the other is fixed, for various sets of variables. The motion of singularities in the case (z, s) shown in Figs. 9 and 14 and Table I indicates the results for all such possible sets of variables.

C. The Blankenbecler-Nambu-Mandelstam Method[14]

To obtain further insight into the origin and nature of these complex anomalous singularities, we consider the fixed $t = 0$ dispersion relation for our box diagram, which in the nonanomalous case (say $z < 0$) is

$$B(s,z) = \frac{1}{2\pi i}\int_{(m_2+m_4)^2}^{\infty} ds' \frac{\mathrm{disc}_s B(s',z)}{s'-s}, \quad t=0. \tag{73}$$

Using Cutkosky's discontinuity formula,[10] assuming a coupling constant g at each vertex in Fig. 8 and defining, at $t=0$, $q_1^2 = q_3^2 \equiv \kappa$, $q_2^2 \equiv \beta$, $q_4^2 = \tau$, $m_1 = m_3 = \mu$, we get

$$\mathrm{disc}_s B(s,z) = \frac{ig^4}{(2\pi)^4}\frac{\pi(-2\pi i)^2}{2[\lambda(s,z,M^2)]^{1/2}}\int_{\beta_{\min}}^{\beta_{\max}} d\beta\,\delta(\beta - m_2^2)\theta(q_2^0)\int_{\tau_{\min}}^{\tau_{\max}} d\tau\,\delta(\tau - m_4^2)\theta(q_4^0)\int_{\kappa_{\min}}^{\kappa_{\max}} d\kappa \frac{1}{(\kappa-\mu)^2}, \tag{74}$$

where $\beta_{\min,\max}$, $\tau_{\min,\max}(\beta)$, and $\kappa_{\min,\max}(\tau,\beta)$ are the extrema relative to q_3^μ when two of the three squared four-momenta are kept fixed. They can be shown[2a,10] to be determined by the Landau equation

$$\alpha_2 q_2^\mu + \alpha_3 q_3^\mu + \alpha_4 q_4^\mu = 0, \tag{75}$$

where the α's serve as Lagrange's undetermined multipliers.

From these equations we determine the integration limits to be as follows:

$$\begin{aligned}
&\beta_{\min} = 0, \quad \beta_{\max} = \infty,\\
&\tau_{\min} = 0, \quad \tau_{\max} = (\sqrt{s} - \sqrt{\beta})^2,\\
&\kappa_{\max,\min}(s,z,M^2;\tau,\beta) = M^2 + \beta - (z - M^2 - s)(\tau - \beta - s)/(2s) \pm [\lambda(s,\beta,\tau)\lambda(s,z,M^2)]^{1/2}/(2s),
\end{aligned} \tag{76}$$

where the triangle function is

$$\begin{aligned}
\lambda(x,y,z) &\equiv x^2 + y^2 + z^2 - 2xy - 2yz - 2zx\\
&= [x - (\sqrt{y} + \sqrt{z})^2][x - (\sqrt{y} - \sqrt{z})^2]
\end{aligned} \tag{77}$$

and the masses of the external legs are

$$p_1^2 = p_4^2 = z, \quad p_2^2 = p_3^2 = M^2. \tag{78}$$

Integrating, we get

$$\mathrm{disc}_s B(s,z) = \frac{-ig^4}{8\pi}\frac{[\lambda(s,m_2^2,m_4^2)]^{1/2}}{f(s,z)}\theta(s - (m_2+m_4)^2), \tag{79}$$

where

$$\begin{aligned}
&f(s,z) \equiv \mu^2[s - s_+(z)][s - s_-(z)] = m_2^2[z - z_+(s)][z - z_-(s)],\\
&s_\pm(z) = m_2^2 + m_4^2 - \frac{(M^2 - m_2^2 - \mu^2)(z - m_4^2 - \mu^2)}{2\mu^2} \pm \frac{1}{2\mu^2}[\lambda(M^2, m_2^2, \mu^2)\lambda(z, m_4^2, \mu^2)]^{1/2},\\
&z_\pm(s) = m_4^2 + \mu^2 - \frac{(M^2 - m_2^2 - \mu^2)(s - m_2^2 - m_4^2)}{2m_2^2} \pm \frac{1}{2m_2^2}[\lambda(M^2, m_2^2, \mu^2)\lambda(s, m_2^2, m_4^2)]^{1/2}.
\end{aligned} \tag{80}$$

If we use this expression for $\mathrm{disc}_s B(s,z)$ without the θ function to define it for all real s, then it is an analytic function of z for fixed real s (though it need not be analytic in s). We can use this to define the analytic continuation of $B(s,z)$, for all z, by varying z and suitably distorting the integration contour to avoid the approaching singularities of $\mathrm{disc}_s B$. As we increase z from small values to a point above its normal threshold cut [i.e., $\mathrm{Im}z=+i\epsilon$, $\mathrm{Re}z>(m_2+\mu)^2$], the path followed by the poles in $\mathrm{disc}_s B$ due to $f(s,z)=0$ is shown in Figs. 15 and 16, and to avoid it we must distort the integration path as shown. The final position of this pole (determined by the fixed z) then determines the anomalous threshold, which, being a solution of a quadratic equation, can be in the complex s plane. The complex-conjugate root of f does not cross the integration contour and so gives no singularity of the amplitude on the physical sheet. If we had increased z to a point below the cut [i.e., $\mathrm{Im}z=-i\epsilon$, $\mathrm{Re}z>(m_2+\mu)^2$], then the anomalous threshold would be in the complex-conjugate position.

By similar techniques one can deduce the single-variable analyticity of the integrated absorptive part,

$$R(z)=\int_{(m_2+m_4)^2}^{\infty} ds'\,\mathrm{disc}_s B(s',z). \tag{81}$$

It is easy to see that the roots of $f(s,z)$ represent the anomalous singularities given by the Landau equations. In the present case of a single-loop box graph at $t=0$, this singularity turns out to be a pole. This is a peculiarity of fixing $t=0$ when $q_1^2=q_2^2$ causes a double pole in the integrand of the Feynman integral. The double pole on the first (κ) integration gives a simple pole, which survives the remaining (τ,β) integrations by successively pinching with the remaining simple poles. For general $t\neq 0$ this singularity is a cut joining the triangle and box branch points of $\mathrm{disc}_s B$.[14c,14d] This cut collapses to a pole when $t\to 0$. We find no such poles on the physical sheet for multilooped Feynman graphs. This is easy to understand if we focus our attention on one momentum loop and lump the remaining integrations together. Then a sufficient condition to get a pole in the final amplitude (irrespective of the sheet it lies on) is that the starting integrand have a double (or higher-order) pole, so that the "first (κ) integration" yields at least a simple pole. Then the integrands for the remaining two (β and τ) integrations must be such that they do not "smooth" this pole into a cut on successive integrations. This requires that these remaining integrands provide pinching poles. Hence only a single-loop Feynman graph at $t=0$, whose four legs are elementary particles $[1/(p^2-m^2+i\epsilon)]$ or resonances $[1/(p^2-m^2+im\Gamma)]$, can, in general, give such anomalous poles.

Using similar arguments one can show that inclusion of spin turns these anomalous poles into a pole plus a cut at the same point, and that inclusion of form factors can "smooth" out these Landau singularities.

For applications to the study of "scaling"[1] of the inelastic structure functions it is convenient to know the analytic structure of $\mathrm{disc}_s B$ for fixed real s in the complex x plane. The Landau singularities of $\mathrm{disc}_s B(s,x)$ are located at

$$x_\pm(s)=z_\pm(s)/[s-M^2-z_\pm(s)] \tag{82}$$

and they move as we vary s. From the above formula we see that when s is large compared to a suitable combination of the internal masses,[11] these singularities $x_\pm(s)$ move rapidly to positions extremely close to their asymptotic position $x_\pm(\infty)$. The rapidity of this approach to the asymptotic region can be deduced from the above equations. In a separate publication[11] we discuss how these observations could provide a possible explanation for a rapid approach to "universality" of the inelastic electron-scattering structure functions. By "universality" we mean that the inelastic structure functions become s-independent functions of x once s is large enough. This is in contrast to "scaling" which requires both s and z to be large before one obtains a function of x alone.

To understand intuitively this explanation of "universality," let us consider the following model of the discontinuity of a box diagram ($t=0$) with spin, for large real s and fixed $x=z/\nu$:

$$\mathrm{disc}_s \tilde{B}(s,x)\equiv\frac{\text{const}}{[\lambda(s,z,M^2)]^{1/2}}\int_0^\infty d\beta\,\delta(\beta-m_2^2)\theta(q_2^0)\int_0^s d\tau\,\delta(\tau-m_4^2)\theta(q_4^0)\int_{\kappa\,\min}^{\kappa\,\max} d\kappa\frac{\kappa}{(\kappa-\mu^2)^2}, \tag{83}$$

where $[\lambda(s,z,M^2)]^{1/2}$ represents the second-type singularity at the edge of the physical region and the factor κ is the effect of spin. Integrating, we get

$$[\lambda(s,z,M^2)]^{1/2}\,\mathrm{disc}_s\tilde{B}(s,x)\propto F(s,x)=\ln\left(\frac{\kappa_{\max}(s,x)-\mu^2}{\kappa_{\min}(s,x)-\mu^2}\right)+\mu^2\left[\frac{1}{\kappa_{\min}(s,x)-\mu^2}-\frac{1}{\kappa_{\max}(s,x)-\mu^2}\right], \tag{84}$$

where, as $s\to\infty$ for fixed finite x,

$$[\kappa_{\min}(s,x)-\mu^2]\to -\frac{\mu^2}{(x+1)}(x+1+s/\mu^2),$$
$$[\kappa_{\max}(s,x)-\mu^2]\to \Sigma_2(x)=\text{a quadratic } s\text{-independent function of } x. \tag{85}$$

This shows that singularities in $F(s,x)$ arise when the edges of the allowed phase space $\kappa_{\max,\min}$ approach the exchanged mass μ^2. For large finite s, the singularity $\kappa_{\min}-\mu^2=0$ is very far (at $x=-1-s/\mu^2$) from the region of interest $-1\leq x\leq 0$ in the complex x plane. On the other hand, the singularities $\kappa_{\max}-\mu^2=0$ are close to the experimental region and s-independent since the edge $\kappa_{\max}$ of the phase space has stopped moving. So, if we assume that the variations with s in the "shape" of the function $F(s,x)$ versus x are controlled by the motion of the nearby singularities, then we should expect F to attain a universal s-independent shape once $\kappa_{\max}(s,x)$ is s-independent. However, the s dependence of the over-all magnitude of $F(s,x)$ is determined by all its singularities and will, in particular, be affected by the distant s-dependent singularity $\kappa_{\min}-\mu^2=0$. In a case (like the above) when this distant singularity is giving a divergent contribution due to ultraviolet divergence in the graph, the magnitude of F will diverge as $s\to\infty$. This is one source of "nonscaling" behavior in certain field-theoretic models of inelastic electron scattering.[1n] The other is the z dependence of the form factors in graphs with vertex corrections. These graphs have "smoother" singularities which, hopefully, give a negligible contribution.

We may choose to adopt the philosophy that the ultraviolet divergences are a disease of the theory rather than of nature, and assume that there exists a realistic causal and unitary S-matrix theory without such divergences. Then we know[3] that the physical-sheet analytic structure (i.e., the position of the singularities but not their nature) obtained from finite-order Feynman perturbation theory (with a cutoff) is expected to be the same as that obtained from this unitary s-matrix theory. In such a theory the experimental data in the region $-1\leq x\leq 0$ should be expected to show the effects of the nearby singularities ($\kappa_{\max}-\mu^2=0$), rather than the effects of the distant singularities ($\kappa_{\min}-\mu^2=0$) which are obtained in the asymptotic models based on summing leading ultraviolet divergences.[1n] This provides the motivation for constructing models[11] of inelastic-electron-scattering structure functions which are based on their analytic structure and dominant singularities.

It is easy to generalize these arguments to arbitrary graphs, and specially those that correspond to a peripheral production of the intermediate state. In this way one can also see why the physical x-sheet singularities correspond to box- or triangle-shaped reduced graphs.

D. Single-Variable Dispersion Relations for the Full VFC Amplitude

As far as dispersion relations[1,2] are concerned, we find that one can always write a fixed real ν_R dispersion relation in z for the amplitude B with integrals over only real contours and real poles, as long as the asymptotic behavior is "decent" enough to be handled by a finite number of subtractions. Also, because of the Sugawara-Kanazawa theorem,[2h,2m,2n] one just needs to check the asymptotic behavior in only one direction in the complex z plane. On the other hand in the case of real s_R fixed above the normal threshold there are complex singularities in z and the above theorems fail. In such cases one can again use the Cauchy theorem to write dispersion-like relations, but now one must include the contribution of the complex cuts. We must also independently check that the contribution from the circle at infinity does in fact vanish, or can be taken into account by a suitable number of subtractions. This can usually be done with the help of a wider class of the maximum-modulus theorems called the Phragmén-Lindelöf theorems.[2m,2n]

To see what happens in a realistic model of the full scattering amplitude, we consider a combination of the s-channel and the u-channel box diagrams of Fig. 17(a) at $t=0$, each of which can be obtained from the other by the simple interchange $\nu\to-\nu$. We will now find that our analysis will give the same analytic structure as expected on the basis of the DGS representation.

The possible physical-sheet Landau singularities for such a combination T are shown in Fig. 17(b) in terms of the complex variables (z,ν). By methods already explained, it is easy to see that the physical-region amplitude is a boundary value of an analytic function of two complex variables. The

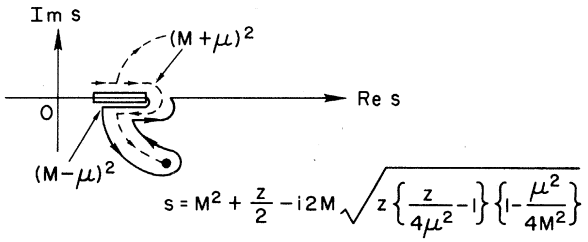

FIG. 15. The motion of the pole in $\mathrm{disc}_s B(s_R,z)$ as z is increased, and the accompanying distortion of the integration contour.

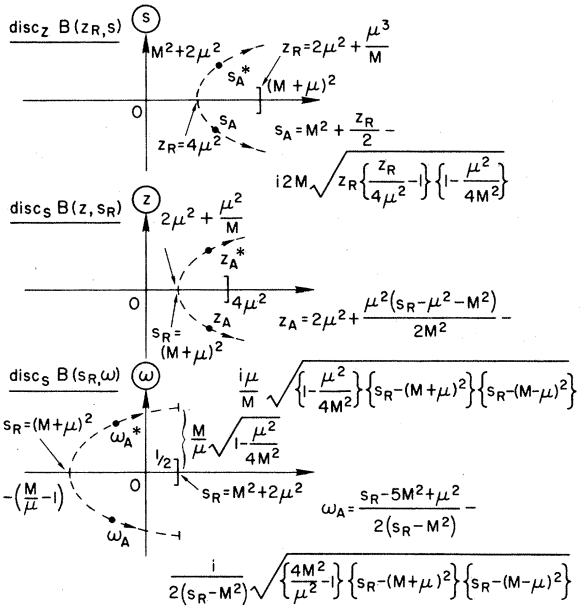

FIG. 16. The single-variable analyticity of disc$_z B(z_R, s)$ in the s plane, of disc$_s B(z, s_R)$ in the z plane, and of disc$_s B(s_R, \omega)$ in the ω plane.

physical boundaries are (Im$z > 0$, Im$\nu > 0$, $\nu > 0$) for the s-channel physical region, and (Im$z > 0$, Im$\nu < 0$, $\nu < 0$) for the u-channel physical region.

We have to be careful when we consider the single-variable analyticity in ν keeping $z = z_R + i\epsilon$ fixed. In such cases the DGS representation for $T(z_R + i\epsilon, \nu)$ indicates a cut along the whole real ν axis when $z_R > \mu^2$. But this does not *a priori* rule out the possibility of finding an analytic continuation in ν with complex singularities but a large domain of analyticity. In fact we saw that such an analytic continuation does exist for the s-channel box diagram. But when we take the amplitude $T(z_R + i\epsilon, \nu)$ to be the combination of the s-channel and the u-channel box graphs, we find that the ν-plane analytic structure is as shown in Fig. 18. We find that for $z > 2\mu M + \mu^2$ the s-channel normal cut Σ_s overlaps the u-channel normal cut Σ_u, and the physical region of the combined amplitude T (which is above the Σ_s cut and below the Σ_u cut when these cuts are chosen parallel to the real ν axis) is squeezed between these two normal cuts and vanishes in the limit $\epsilon \to 0+$. Clearly, under such circumstances we cannot determine the physical value of the amplitude as the boundary value of such an analytic continuation in one complex variable. One way to rectify this situation would be to define a different analytic continuation by distorting the cuts, but then we would risk exposing the singularities on the unphysical sheet, since during the deformation of the cuts these unphysical singularities could cross through onto the

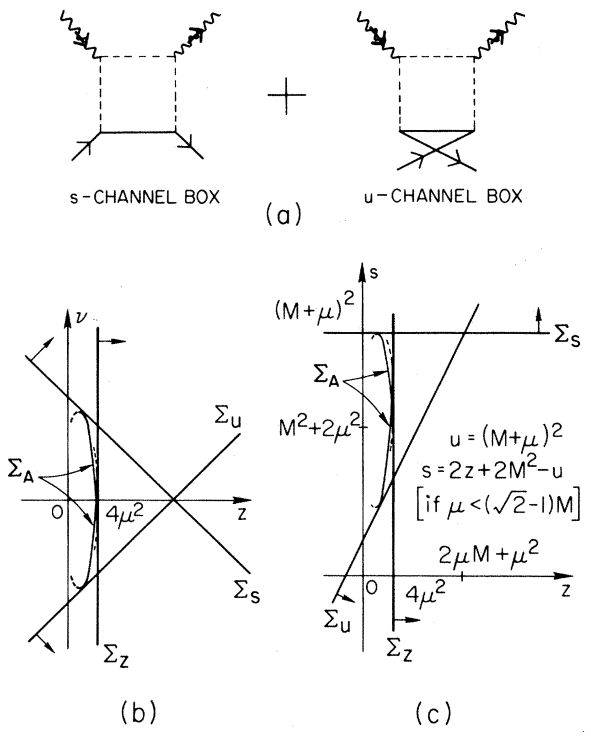

FIG. 17. The analytic structure of the sum of direct- and crossed-channel box diagrams.

physical sheet. The other choice is to consider an analytic continuation in ν which is separated by a cut along the whole real ν axis, the s-channel physical region being just above this cut and the u-channel physical region just below. This, we would observe, is precisely what happens in the case of the DGS representation. On the other hand, if we fix $\nu = \nu_R$, and Im$\nu = 0$ and consider the analyticity in z, we find that we do get a real analytic function of z for any ν in spite of the u-channel cuts, and that the physical boundary of this real analytic function of one complex variable is Im$z > 0$, i.e., $z = z_R + i\epsilon$. The location of the physical

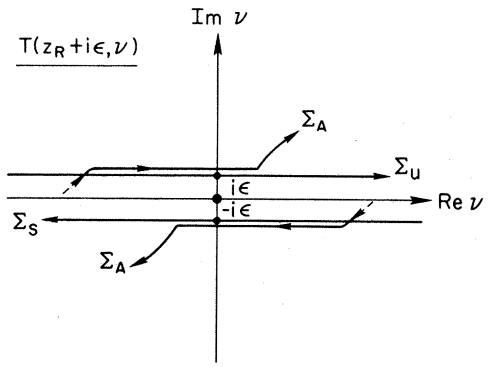

FIG. 18. The single-variable analytic structure of $T(z_R + i\epsilon, \nu)$ in the ν plane, showing the overlap of the normal cuts.

boundary is most easily deduced from the expressions for the imaginary parts of the denominators in the Nambu representation of the s- and u-channel box diagrams. These are, respectively, of the form

$$\begin{aligned}\mathrm{Im}D_{(s)} &= (a+b)\mathrm{Im}z + b\mathrm{Im}\nu + c \\ &= a\mathrm{Im}z + b\mathrm{Im}s + c \end{aligned} \tag{86}$$

and

$$\begin{aligned}\mathrm{Im}D_{(u)} &= (a+b)\mathrm{Im}z - b\mathrm{Im}\nu + c \\ &= (2b+a)\mathrm{Im}z - b\mathrm{Im}s + c, \end{aligned} \tag{87}$$

where $a>0$, $c>0$, $b\geq 0$, and $\epsilon \to 0+$.

If we consider the pair of variables (z, s) we find that we run again into the problem of overlapping cuts in the complex s plane if we fix $z = z_R + i\epsilon$ with $z_R > 2\mu M + \mu^2$. At $z_R > 4\mu^2(1 - \mu^2/4M^2)$ this function ceases to be real analytic in s because of the anomalous thresholds. Similarly, if we fix $s = s_R$ and $\mathrm{Im}s = 0$, we get a real analytic function of z only if $s < (M+\mu)^2$.

From this discussion we conclude that for the full forward Compton scattering amplitude we cannot expect much more single-variable analyticity than that implied by the DGS representation and shown in Table I.

V. THE ANALYTIC STRUCTURE OF DISCONTINUITIES AND INELASTIC STRUCTURE FUNCTIONS

The two-variable analyticity of the amplitude $T(s, z)$ implies a single-variable analyticity of the difference $T(s_1, z) - T(s_2, z)$ in the complex z plane if we keep s_1 and s_2 fixed. Cutkosky[10] used this fact, in the framework of Feynman perturbation theory, to determine the single-variable analyticity of the discontinuities of the amplitude across fixed cuts. He showed that the singularities of a given Feynman integral $F(\xi)$, which are also the singularities of the discontinuity $F_m(\xi)$ (across the cut due to the reduced graph with m legs on the mass shell), are those which correspond to the (reduced and full) Landau diagrams, in which lines have been added to the given reduced diagram which defined the original singularity. The other Landau singularities of $F(\xi)$ appear on both sheets (corresponding to the given fixed cut) and their cuts cancel when we calculate the difference. The singularities of F which correspond to the reduced graphs with additional internal lines i ($i>m$ on the mass shell) appear on only one of the two adjacent sheets connected by the branch point corresponding to the reduced graph with m lines on the mass shell (e.g., the anomalous threshold due to triangle graphs moves from the second to the first sheet of the normal thresholds due to bubble graphs). This discontinuity can also carry the non-Landau singularities. These facts can readily be seen from the structure of the Cutkosky formula for calculating discontinuities (remembering that in applying this formula one integrates in the physical region and then analytically continues into the unphysical domain). This formula can also be used to calculate the discontinuity $F_{m,m'-m}(\xi)$ of the discontinuity function $F_m(\xi)$ across a (fixed) cut corresponding to a reduced graph in which the additional internal lines i ($m<i\leq m'$) are also on the mass shell, and we find that

$$F_{m,m'-m} \equiv F_{m'} = (-2\pi i)^{m'} \int\cdots\int \frac{\prod_{\text{loops}} d^4k\, \delta(q_1^2 - \mu_1^2)\theta(q_1^0)\cdots \delta(q_{m'}^2 - \mu_{m'}^2)\theta(q_{m'}^0)}{(q_{m'+1}^2 - \mu_{m'+1}^2)\cdots(q_N^2 - \mu_N^2)} \tag{88}$$

[the sign of $F_{m,m'-m}(\xi)$ is, in fact, defined by this relation]. This result can be obtained by the following replacement in the original Feynman integral:

$$\frac{1}{(q^2-\mu^2)^{r+1}} \to \frac{(-2\pi i)\theta(q^0)}{r!}\frac{d^r}{d(\mu^2)^r}\delta(q^2-\mu^2). \tag{89}$$

The Cutkosky formula defines an analytic function of the internal masses and external invariants, whose domain of analyticity must be found by analytic continuation. This, in general, could be a very difficult problem. But in the special case when we are interested in the single-variable analyticity in the second variable of the discontinuity across a fixed cut in the first variable (like the normal s-threshold cut) the problem is much simpler. Then it only requires the knowledge of the ordinary and virtual anomalous singularities on the physical sheet of the second variable (like the complex z plane). This will become clear from our discussion and Cutkosky's analysis. In practice we are interested in the various boundary values of this function. For example, $\mathrm{disc}_s T(z_R + i\epsilon, s_R)$ across only the normal s cut is one such boundary value above the real z cut, which corresponds to giving all internal masses a small negative imaginary part when one starts to encounter singularities on the real axis. (This is because $\mathrm{disc}_s T$ is of the form T^2.) These small imaginary parts are inessential on the cut-free region of the real axis. On the other hand we observe, from their definition, that the inelastic structure functions are a different boundary value, whose boundary is discovered by the prescription of putting $m_i^2 \to m_i^2 - i\epsilon$ for the internal masses in the initial state and $m_f^2 \to m_f^2 + i\epsilon$ for the internal masses in the final

state, when one encounters real singularities. (This is because they are of the form $|T|^2$.) The mixed nature of this prescription makes it difficult to determine the boundary for arbitrary graphs.[7c,10] But in the regions of the real axis where the discontinuities are cut-free (and pure imaginary) the $\pm i\epsilon$ are irrelevant, so that their values will agree (up to factors of i) with those of the various inelastic structure functions defined by a similar formula, even though the imaginary part of the amplitude in this region is a sum of different discontinuities across various cuts and not a boundary value of any discontinuity function. This follows from the conjugate symmetry $[T^*(s^*, z^*) = T(s, z)]$ of the VFC amplitude, from which we see that

$$\begin{aligned}\mathrm{disc}_s T(s_R, z) &\equiv T(s_R + i\epsilon, z) - T(s_R - i\epsilon, z) \\ &= -[\mathrm{disc}_s T(s_R, z^*)]^*. \end{aligned} \tag{90}$$

Hence, on the cut-free part of the real z axis we can reach the point $z^* = z = z_R$ where

$$\begin{aligned}\mathrm{disc}_s T(s_R, z_R) &= -[\mathrm{disc}_s T(s_R, z_R)]^* \\ &= \text{pure imaginary}. \end{aligned} \tag{91}$$

This is not possible on parts of the real z axis lying inside a cut. Similarly we find that

$$\begin{aligned}2i\mathrm{Im}T(s_R + i\epsilon, z_R + i\epsilon) &= [\mathrm{disc}_s T(s_R, z_R + i\epsilon)]^* \\ &\quad - \mathrm{disc}_z T(s_R + i\epsilon, z_R). \end{aligned} \tag{92}$$

In this formula $\mathrm{disc}_s T$ represents the contribution of the connected direct-channel graphs of Fig. 3(b), while $\mathrm{disc}_z T$ gives the contribution of the semidisconnected graphs of Fig. 3(d), to the total imaginary part of the VFC amplitude. Since by definition $\mathrm{Im}T(s_R + i\epsilon, z_R + i\epsilon)$ must be real, hence

$$\begin{aligned}\mathrm{Re}[\mathrm{disc}_s T(s_R, z_R + i\epsilon)] &= \mathrm{Re}[\mathrm{disc}_z T(s_R + i\epsilon, z_R)] \\ &= \tfrac{1}{2}\mathrm{disc}_z[\mathrm{disc}_s T(s_R, z_R)], \end{aligned} \tag{93}$$

which is related to the imaginary part that the inelastic-electron-scattering structure functions develop due to the presence of the double-discontinuity graphs (like the semidisconnected graphs) when we try to continue the structure function to the annihilation region (where z is timelike).

Thus we see why a simple relation between the discontinuities or the structure functions and the imaginary parts of the amplitude only holds in cases when the amplitude is real analytic $[T^*(s^*, z) = T(s, z)]$, rather than when it is conjugate symmetric $[T^*(s^*, z^*) = T(s, z)]$.

Using the Cutkosky formula, we can identify $\mathrm{disc}_s T$, $\mathrm{disc}_u T$, and $\mathrm{disc}_z T$, on their cut-free sections of the real axes, with the non-Born-term parts of the structure functions $C(s, z)$, $P(u, z)$, and $D(z, s)$, respectively. The conventional functions W and $\overline{W}$ are trivially related to C and P, respectively. The Born terms give nonanalytic δ-function contributions to C, P, and D.

To understand the main features of the analytic structure of the discontinuities, we first consider the example of $\mathrm{disc}_s B$. This was explicitly evaluated in the last section. We leave the detailed discussion of higher orders to a subsequent publication. We find from this calculation that for fixed real $s_R > (m_2 + m_4)^2$, $\mathrm{disc}_s B(s_R, z)$ is analytic in the whole z plane except for a pair of anomalous singularities at $f(s_R, z) = 0$. For $s_R < (m_2 + m_4)^2$, $\mathrm{disc}_s B(s_R, z) = 0$. Since $\mathrm{disc}_s B(s_R, z)$ is not required to be analytic in s_R, this sudden disappearance of anomalous singularities for $s_R < (m_2 + m_4)^2$ should not be surprising. When $\lambda(M^2, m_2^2, \mu^2) < 0$ (Euclidean case) the anomalous singularities are at complex-conjugate points $z_\pm(s)$. When $\lambda(M^2, m_2^2, \mu^2) > 0$ (non-Euclidean case) the anomalous singularities consist of a pair of virtual anomalous singularities on the real axis. We note that there are no cuts along the real z axis in $\mathrm{disc}_s B(s_R, z)$, even though $B(s_R, z)$ does have a cut $(m_4 + \mu)^2 \leq z \leq \infty$. This just reflects the fact that $\mathrm{disc}_s B(s_R, z)$ must only contain ordinary and virtual singularities of B which correspond to adding lines to the reduced graphs defining $\mathrm{disc}_s B$. It could have real cuts for $z > 0$ if the virtual singularities were branch points, or if it had vertex corrections as in the graphs of Fig. 19. The real cuts would join the pairs of virtual branch points and extend to infinity from normal threshold branch points.

For fixed z_R the above formula of $\mathrm{disc}_s B(s_R, z_R)$ was used without the θ function to define it for all s, and we noticed that it had both the s-channel normal threshold branch points (instead of only one like the amplitude). This is easily understood by the fact that in trying to analytically continue this formula to s below $(m_2 + m_4)^2$, we necessarily cross over into the unphysical sheet in the s plane of one of the amplitudes $B(s_R \pm i\epsilon, z_R)$, and therefore as a function of s the $\mathrm{disc}_s B$ necessarily exposes the singularities on both the physical and the adjacent unphysical sheet. This is also seen from the definition

$$\mathrm{disc}_s B = B_{\mathrm{II}s} - B_{\mathrm{I}s}, \tag{94}$$

where the numerical subscripts denote the sheet of the normal s-threshold cut. We see that $\mathrm{disc}_s B$ must carry the singularities of both the first and the second s sheets. This complicates the study of its analyticity in the complex s plane, and that is why we restrict ourselves to the complex z plane keeping s fixed.

Keeping ν fixed also complicates the analytic structure in the complex z plane, since

$$\mathrm{disc}_{\nu} B(\nu_R, z) = \mathrm{disc}_{s} B(s_R - z_R - M^2, z). \tag{95}$$

From this relation it is clear that the analyticity of this function cannot be simply related to the single-variable analyticity of any amplitude, since for fixed ν_R, complexifying z requires simultaneous complexification of s_R and, as indicated above, this exposes all the singularities on the unphysical sheet of the s plane, all of which are not known to us. Besides the Landau singularities, the unphysical s sheets can carry the second-type singularities and also the singularities which come from the divergence of the sum of the perturbation series.[15]

Thus great care must be exercised when discussing the single-variable analytic continuations of the discontinuities across moving branch cuts, to make sure that the analytic continuations are meaningful (that is, there exists a reason for the discontinuity to be an analytic function of one variable), and that the singularities coming from the unphysical sheets of the amplitude are correctly taken into account.

We should, however, observe that since the discontinuities across given fixed normal cuts do not have these normal branch points, the inclusion of crossed-channel diagrams does not affect their single-variable analyticity, as it did for the amplitude.

To summarize, we find that in general $\mathrm{disc}_s T(s_R, z)$, $\mathrm{disc}_u T(u_R, z)$, and $\mathrm{disc}_z T(z_R, s)$ across the respective fixed normal s, u, or z threshold cuts are analytic functions of the second complex variable when we fix s, u, or z, respectively, at real values. Besides the real normal

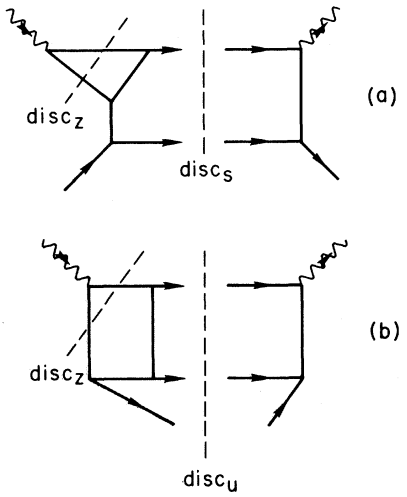

FIG. 19. Typical double-discontinuity graphs leading to real cuts in the discontinuity functions.

threshold cuts (coming from double-discontinuity graphs like those of Fig. 19) they carry the ordinary (complex) and virtual (real) anomalous singularities. On the other hand, the non-Born-term parts of the inelastic structure functions $C(s_R, z)$, $P(u_R, z)$, and $D(z_R, s)$ are boundary values of these discontinuity functions, respectively, on and only on the cut-free part of the real axis.

Since there are no real singularities for spacelike $z_R < 0$, the non-Born-term part of the inelastic-electron-scattering structure function $W^{\mathrm{NB}}(s_R, z_R)$ [or $C(s_R, z_R)$] for fixed real s_R is a boundary value on the real z axis of an analytic function in the experimentally accessible region $z_R < 0$. This is not true in general for timelike $z_R > 0$, due to the presence of double-discontinuity graphs (like Fig. 19) causing real cuts in the region $z_R > 0$, and due to the presence of real virtual anomalous singularities. If, however, for some dynamical reason the contribution of the double-discontinuity graphs (like the semidisconnected graphs) vanishes, and the real cut joining the pairs of virtual anomalous singularities lies out of the timelike region of interest, then in this cut-free timelike region the $W^{\mathrm{NB}}(s_R, z_R)$ is again a boundary value of an analytic function. An example of such a dynamical reason[1c,11] is the transverse momentum cutoff and $s \to \infty$ limit in the Drell-Levy-Yan model, which causes graphs like those of Fig. 21 to give a vanishing contribution.

As far as the complex part of the z plane of $\mathrm{disc}_s T(s_R, z)$ is concerned, we find from the formula for $z_{\pm}(s)$ that the complex anomalous box singularities move towards the right ($\mathrm{Re}z > 0$) or left ($\mathrm{Re}z < 0$) half plane depending on whether $(M^2 - m_2^2 - \mu^2)$ is negative or positive. For a single-loop Feynman graph, baryon conservation requires $(M^2 - m_2^2 - \mu^2)$ to be negative, so that the left half z plane is singularity-free. This inequality is even stronger for box singularities from multilooped Feynman graphs (Fig. 20), since m_2 and μ now represent the sum of the masses of the reduced legs $\sqrt{\beta}$ and $\sqrt{\kappa}$, respectively. Thus one is justified in expanding W^{NB} as a Taylor series in z for fixed real s in the region $\mathrm{Re}z < 0$.[1h]

As an interesting application of these ideas, we study whether we can use the general crossing relation between the inelastic-electron-scattering structure function W and the annihilation structure function $\overline{W}$ to relate inelastic electron scattering to annihilation.[1c] Crossing implies that

$$W(s = u, \omega) = \pm \overline{W}(u = s, -\omega), \tag{96}$$

where the Pauli principle gives positive sign for scattering off bosons and negative sign for scattering off fermions. The inelastic-electron-scattering experiments measure $W(s, \omega)$ for

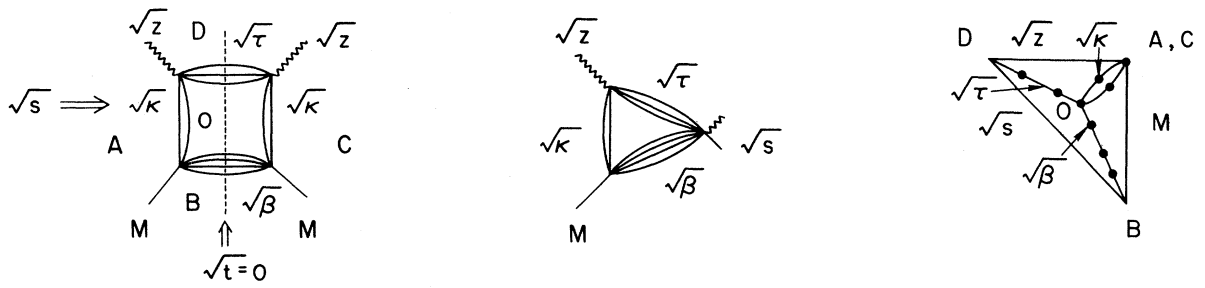

FIG. 20. Typical reduced Feynman graphs leading to an anomalous box or triangle singularity at $t=0$ and the corresponding "tautened" dual diagram.

$s>(m_2+m_4)^2$ and $1<\omega<+\infty$, while for the annihilation cross section we need $\overline{W}(u,\omega)$ for $u>(m_2+m_4)^2$ and $-1<\omega<0$, which can be obtained from the crossing relation if we know $W(s=u,\omega)$ for $s>(m_2+m_4)^2$ and $0<\omega<1$. But, for a general graph, $\mathrm{disc}_s T(s,\omega)$ for fixed real s has a normal threshold (real) cut $\omega_{\mathrm{th}}\leq\omega\leq+1$, together with real cuts joining pair of virtual anomalous singularities that lie in the region $\omega\leq+1$. Therefore, in general the boundary value (above the cut) of $\mathrm{disc}_s T(s,\omega)$ for fixed real s does not represent $W^{\mathrm{NB}}(s,\omega)$ in the region $\omega\leq+1$ owing to the presence of real cuts, and so the crossing relation cannot be used.

However, if the amplitude T is restricted to the class of t-channel ladders with point couplings[1c,1n] (corresponding to a multiperipheral production of intermediate states), then $\mathrm{disc}_s T$ is free from the normal threshold cuts in ω. One still has the real cuts connecting the virtual singularities in the region $\omega<+1$, but these generally lie at a finite distance away from $\omega=+1$. Under such conditions we obtain a cut-free interval from $\omega_c<\omega<\infty$ with $\omega_c<1$, where the boundary value of $\mathrm{disc}_s T$ gives $C(s,\omega)$. We can therefore use crossing to obtain $P(u=s,\omega)$ in the limited region $-1\leq\omega<-\omega_c$. This result for finite energies is the analog of the result obtained by Drell, Levy, and Yan[1c,1l] for asymptotic energies. On the other hand, we find no reason at finite energies for the analyticity conjectured by Pestieau and Roy.[1b]

Further discussion of the analytic structure of the discontinuities and the inelastic structure function will be undertaken in separate publications. There we will use the method of dual diagrams[8] to generalize the analysis to all orders of Feynman perturbation graphs at $t=0$, and show that the only Landau singularities that appear on the physical sheet of the complex z plane for fixed $s=s_R\pm i\epsilon$ (or vice versa) are the s-independent normal z-threshold branch points (for real timelike $z>0$) and a set of anomalous singularities $z_\pm(s)$, which move with s, and correspond to the single-loop box or triangle reduced diagrams. Their equation is given by

$$z_\pm(s)=\tau+\kappa-(M^2-\beta-\kappa)(s-\tau-\beta)/(2\beta)\pm[\lambda(M^2,\beta,\kappa)\lambda(s,\tau,\beta)]^{1/2}/(2\beta), \tag{97}$$

where β, τ, and κ are the squares of the sum of the masses of the bottom, top, and vertical reduced legs, respectively, as shown in Fig. 20.

In the case (Euclidean) in which the lower vertex is internally and externally stable, $\lambda(M^2,\beta,\kappa)<0$ and the $z_\pm$'s represent a pair of complex-conjugate ordinary anomalous Landau singularities when $\lambda(s,\tau,\beta)>0$ [i.e., $s>(\sqrt{z}+\sqrt{\beta})^2$]. On the other hand, in the case (pseudo-Euclidean) in which $\lambda(M^2,\beta,\kappa)>0$, the $z_\pm$'s represent a pair of virtual anomalous singularities on the timelike part of the real x axis. The physical z sheet is defined

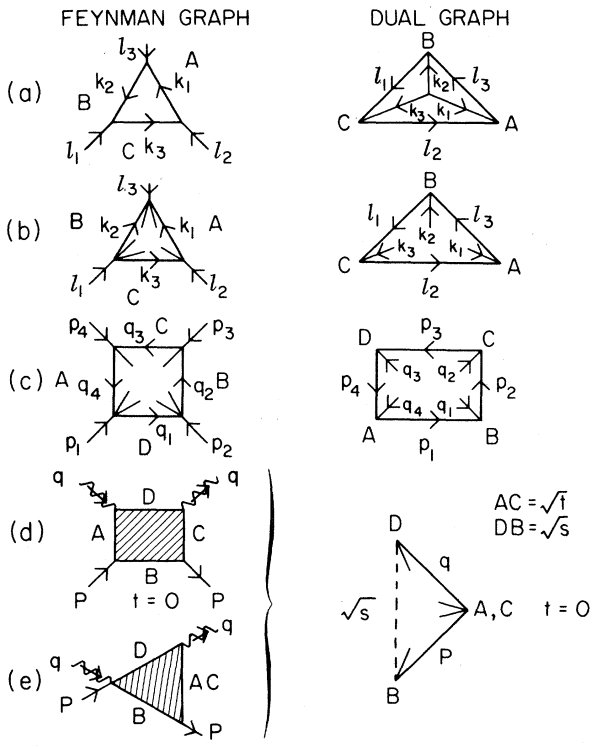

FIG. 21. The dual diagrams for Feynman graphs representing scattering amplitudes and vertex functions.

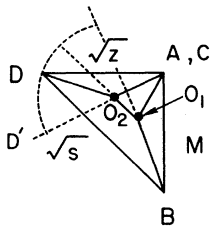

FIG. 22. Typical possible dual diagram for leading singularities of the VFC amplitude.

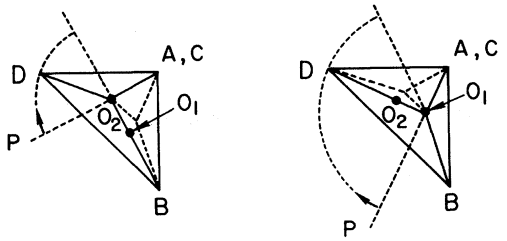

FIG. 23. Dual diagrams of one-order-lower singularities. P represents the point of "effective touch."

to be the sheet of the normal z-threshold cuts (or the lowest-order Landau singularities) that carries the physical boundary. The box and triangle singularities are coincident at $t=0$.

These facts follow[2c,6,8] from the following consequences of the Landau equations and four-momentum conservation:

(1) The dual diagram for the VFC amplitude ($t=0$) has to be drawn in a two-dimensional plane and is triangular (Figs. 20 and 21).

(2) A two-dimensional dual diagram with l internal dual vertices (corresponding to l independent loop momenta), and N internal dual prongs (corresponding to N different internal line momenta), must satisfy $N \leq 2l+1$ to give a nontrivial solution of the Landau equations.

(3) A p-pronged internal dual vertex must be drawn in a $(p-1)$-dimensional space. Each prong could consist of multiple internal lines like OA and OC in Fig. 20. This condition is called "tautening" of the dual diagram. The only anomalous singularities found on the physical sheet are the ones which can climb onto this sheet through the normal threshold cuts, or through the cuts attached to the branch points which have previously come onto the physical sheet through the normal thresholds. The sufficient condition[2a,2c,6] for one Landau singularity to change sheets by moving through the cut attached to another Landau singularity, is that their Landau curves "touch effectively" (or intersect critically). This need not be a necessary condition if we have acnodes or cusps, in the Landau curves. Here we assume their absence.[13]

For two Landau curves to "touch effectively," they must touch and at the point of the touch must have identical values for *all* the Feynman parameters α. It is easy to see that, in the Euclidean region, for two Landau curves to touch, the dual diagram of the higher-order singularity at the point of touch must simultaneously form the dual diagram for the lower-order singularity being touched. For this reason the leading singularity of Fig. 22 cannot touch the one-order-lower singularities of Fig. 23. This geometric criterion for touching is sufficient for our proof, since Landau and Okun and Rudin have shown that in a theory with stable internal lines the multilooped reduced graphs with dual diagrams like in Fig. 22 give leading singularities in the Euclidean region only. Only the single-loop reductions can give singularities in both the Euclidean (ordinary) and the pseudo-Euclidean (virtual) regions.[8] For the examples of Figs. 22 and 23, the leading singularity of Fig. 22 cannot touch the one-order-lower singularity of Fig. 23 because of the tautening of the internal dual vertex O_1 (or O_2). On the other hand, it can touch the two-orders-lower singularity at $z=(DO_2+O_2A)^2$, but this touch is not effective if M is stable so that $0<AO_1B<\pi$. For it to be effective we need $\alpha_{O_1O_2}=0$, which cannot happen if the above condition is satisfied by the angle AO_1B. This just reflects the fact that the reduced diagram corresponding to the O_1O_2 line being absent cannot be singular unless both z and M^2 are simultaneously unstable. On the other hand, the lower-order singularity corresponding to a single-loop reduction of Fig. 23 can come onto the physical sheet at P through the normal z-threshold cut.

We wish to thank R. Blankenbecler, J. D. Bjorken, S. D. Drell, M. Nauenberg, K. G. Wilson, M. Einhorn, R. Haymaker, and T.-M. Yan for very fruitful discussions.

---

*Work supported in part by the U. S. Atomic Energy Commission.

[1](a) H. Abarbanel, M. L. Goldberger, and S. B. Treiman, Phys. Rev. Letters 22, 500 (1969). (b) J. Pestieau and P. Roy, Phys. Letters 30B, 483 (1969). (c) S. D. Drell, D. J. Levy, and T.-M. Yan, Phys. Rev. Letters 22, 744 (1969); Phys. Rev. 187, 2159 (1969); Phys. Rev. D 1, 1035 (1970); 1, 1617 (1970); S. D. Drell and T.-M. Yan, SLAC Report No. SLAC-PUB-808 (unpublished). (d) J. D. Bjorken, Phys. Rev. 179, 1547 (1969). (e) R. Chanda, S. Sen, and D. P. Majumdar, University of Maryland Report No. NYO-3399-217 (SU-1206-217), 1969 (unpublished). (f) J. M. Cornwall, D. Corrigan, and R. E. Norton, Phys. Rev. Letters 24, 1141 (1970); and UCLA report, 1970 (unpublished); R. Jackiw, R. Van Royen, and G. West, Phys. Rev. D 2, 2473 (1970); V. N. Gribov,

Proceedings of the Fourth Winter Seminar on the Theory of the Nucleus and the Physics of High Energies, 1969 (A. F. Ioffe Institute of Engineering Physics, Acad. Sci. USSR, Leningrad). (g) T. P. Cheng and Wu-Ki Tung, Phys. Rev. Letters 24, 851 (1970). (h) M. Nauenberg, Phys. Rev. Letters 24, 625 (1970). (i) J. J. Sakurai, *Currents and Mesons* (University of Chicago Press, Chicago, 1969). (j) J. D. Sullivan, University of Illinois, Urbana, report, 1970 (unpublished). (k) W. T. Potter and J. D. Sullivan, CERN Report No. CERN-TH-1213, 1970 (unpublished). (l) P. V. Landshoff, CERN Report No. CERN-TH-1154, 1970 (unpublished). (m) S. L. Adler and R. F. Dashen, *Current Algebras* (Benjamin, New York, 1968). (n) S. J. Chang and P. M. Fishbane, Phys. Rev. Letters 24, 874 (1970).

[2](a) R. J. Eden, P. V. Landshoff, D. I. Olive, and J. C. Polkinghorne, *The Analytic S Matrix* (Cambridge University Press, New York, 1966), and references therein. We will refer to this book as ELOP. (b) R. J. Eden, *High Energy Collisions of Elementary Particles* (Cambridge University Press, New York, 1967). (c) R. J. Eden, in *1961 Brandeis University Summer Institute in Theoretical Physics,* edited by K. W. Ford (Benjamin, New York, 1962); J. C. Polkinghorne, *ibid.*, p. 102. (d) *Dispersion Relations,* Scottish Universities' Summer School, edited by G. R. Screaton (Oliver and Boyd, Edinburgh, Scotland, 1961). (e) J. D. Bjorken and S. D. Drell, *Relativistic Quantum Fields* (McGraw-Hill, New York, 1965). (f) P. V. Landshoff, in *Dispersion Relations and Their Connection with Causality, Proceedings of the International School of Physics "Enrico Fermi," Course XXIX,* edited by E. P. Wigner (Academic, New York, 1964). (g) K. Nishijima, *Fields and Particles* (Benjamin, New York, 1969). (h) G. Barton, *Introduction to Advanced Field Theory* (Interscience, New York, 1963), and *Dispersion Techniques in Field Theory* (Benjamin, New York, 1965). (i) L. Klein, *Dispersion Relations and Abstract Approach to Field Theory* (Gordon and Breach, New York, 1961). (j) R. Hagedorn, *Introduction to Field Theory and Dispersion Relations* (Macmillan, New York, 1964). (k) R. F. Streater and A. S. Wightman, *PCT, Spin and Statistics and All That* (Benjamin, New York, 1964). (l) A. O. Barut, *The Theory of the Scattering Matrix for the Interactions of Fundamental Particles* (Macmillan, New York, 1967). (m) E. C. Titchmarsh, *The Theory of Functions* (Oxford University Press, London, 1961). (n) E. Hille, *Analytic Function Theory* (Ginn and Company, New York), Vol. I, 1959; Vol. II, 1962.

[3]J. C. Polkinghorne, Nuovo Cimento 23, 360 (1962); 25, 901 (1962); Phys. Rev. 128, 2459 (1962); 128, 2898 (1962); and Ref. 2(a), Secs. 4.1, 4.10, and 4.11.

[4](a) S. Deser, W. Gilbert, and E. C. G. Sudarshan, Phys. Rev. 115, 731 (1959); 117, 266 (1960); 117, 272 (1960). (b) M. Ida, Progr. Theoret. Phys. (Kyoto) 23, 1151 (1960). (c) N. Nakanishi, Progr. Theoret. Phys. (Kyoto) Suppl. 18, 1 (1961), Sec. 16; Progr. Theoret. Phys. (Kyoto) 26, 337 (1961); 26, 927 (1961); J. Math. Phys. 3, 1139 (1962); Phys. Rev. 127, 1380 (1962); J. Math. Phys. 4, 1385 (1963); 5, 1458 (1964). (d) J. M. Cornwall and R. E. Norton, Phys. Rev. 173, 1637 (1968); 177, 2548 (1969). (e) B. Schroer and P. Stichel, Commun. Math. Phys. 3, 258 (1966). (f) R. Jost and H. Lehmann, Nuovo Cimento 5, 1598 (1957). (g) F. J. Dyson, Phys. Rev. 110, 1460 (1958). (h) We would like to thank Dr. M. B. Einhorn and Dr. M. J. Creutz for some very useful discussions about the DGS representation. (i) J. Schwinger, Phys. Rev. Letters 3, 296 (1959). (j) K. Johnson, Nucl. Phys. 25, 431 (1961). (k) L. S. Brown, in *Boulder Lectures in Theoretical Physics, 1969,* edited by W. E. Brittin, B. W. Downs, and J. Downs (to be published).

[5](a) S. D. Drell and J. D. Walecka, Ann. Phys. (N. Y.) 28, 18 (1964). (b) M. Gourdin, Nuovo Cimento 21, 1094 (1961).

[6](a) N. Nakanishi, Progr. Theoret. Phys. (Kyoto) Suppl. 18, 1 (1961). (b) J. S. R. Chisholm, Proc. Cambridge Phil. Soc. 48, 300 (1952). (c) T. Appelquist, Ann. Phys. (N. Y.) 54, 27 (1969). (d) R. J. Eden, Phys. Rev. 119, 1763 (1960); 121, 1567 (1961). (e) R. J. Eden, P. V. Landshoff, J. C. Polkinghorne, and J. C. Taylor, Phys. Rev. 122, 307 (1961). (f) P. V. Landshoff, Phys. Letters 3, 116 (1962). (g) J. Cunningham, Rev. Mod. Phys. 36, 833 (1964). (h) P. V. Landshoff, J. C. Polkinghorne, and J. C. Taylor, Nuovo Cimento 19, 939 (1961). (i) E. S. Sarachik, Nuovo Cimento 51A, 949 (1967). (j) J. Tarski, J. Math. Phys. 1, 149 (1960). (k) L. F. Cook and J. Tarski, J. Math. Phys. 3, 1 (1962); Phys. Rev. Letters 5, 585 (1960). (l) D. Bessis and F. Pham, J. Math. Phys. 4, 1253 (1963). (m) R. E. Norton, Phys. Rev. 135, B1381 (1964). (n) P. Collas and R. E. Norton, Phys. Rev. 160, 1346 (1967). (o) S. Coleman and R. E. Norton, Nuovo Cimento 38, 438 (1965). (p) G. Barton and C. Kacser, Nuovo Cimento 21, 593 (1961); 21, 1001 (1961).

[7](a) R. Blankenbecler and J. Tarski, Phys. Rev. 125, 782 (1962). (b) J. D. Bjorken and J. D. Walecka, Ann. Phys. (N. Y.) 38, 35 (1966). (c) I. T. Drummond, Nuovo Cimento 24, 248 (1962); 29, 720 (1963).

[8](a) L. D. Landau, Nucl. Phys. 13, 181 (1959). (b) L. B. Okun and A. P. Rudik, Nucl. Phys. 14, 261 (1960). (c) M. Fowler, J. Math. Phys. 3, 936 (1962). (d) P. V. Landshoff, Nucl. Phys. 20, 129 (1960). (e) J. C. Taylor, Phys. Rev. 117, 261 (1960). (f) Refs 2(c) and 2(d).

[9](a) D. B. Fairlie, P. V. Landshoff, J. Nuttall, and J. C. Polkinghorne, J. Math. Phys. 3, 594 (1962); Phys. Letters 3, 55 (1962). (b) P. Federbush, J. Math. Phys. 6, 825 (1965).

[10]R. E. Cutkosky, J. Math. Phys. 1, 429 (1960); Phys. Rev. Letters 4, 624 (1960).

[11]Ashok suri, Phys. Rev. Letters 26, 208 (1971).

[12](a) C. Fronsdal, K. Mahanthappa, and R. E. Norton, Phys. Rev. 127, 1847 (1962); J. Math. Phys. 4, 859 (1963). (b) J. N. Islam, J. Math. Phys. 3, 1098 (1962).

[13](a) R. J. Eden, P. J. Landshoff, J. C. Polkinghorne, and J. C. Taylor, J. Math. Phys. 2, 656 (1961). (b) D. I. Olive and J. C. Taylor, Nuovo Cimento 24, 814 (1962). (c) J. N. Islam, J. Math. Phys. 4, 872 (1963). (d) N. Nakanishi, J. Math. Phys. 4, 1539 (1963).

[14](a) R. Blankenbecler and Y. Nambu, Nuovo Cimento 18, 595 (1960). (b) S. Mandelstam, Phys. Rev. Letters 4, 84 (1960); Phys. Rev. 115, 1741 (1959). (c) V. N. Gribov, M. V. Terent'ev, and K. A. Ter-Martirosyan, Zh. Eksperim. i Teor. Fiz. 40, 337 (1961) [Soviet Phys. JETP 13, 229 (1961)]. (d) R. Oehme, Nuovo Cimento 13, 778 (1959). (e) G. Wanders, Nuovo Cimento 17, 535 (1960); 18, 580 (1960). (f) R. C. Brunet, University of Montreal report, 1970 (unpublished).

[15]R. Blankenbecler, private communications. See also Refs. 2(a) and 3.